LiNbO$_3$ Y-BRANCH OPTICAL MODULATOR

by

WINNIE CHELSEA LAI

B. A. Sc. (Hons), The University of British Columbia, 1988

A THESIS SUBMITTED IN PARTIAL FULFILMENT OF

THE REQUIREMENTS FOR THE DEGREE OF

MASTER OF APPLIED SCIENCE

in

THE FACULTY OF GRADUATE STUDIES

(The Department of Electrical Engineering)

We accept this thesis as conforming

to the required standard

THE UNIVERSITY OF BRITISH COLUMBIA

September 1991

In presenting this thesis in partial fulfilment of the requirements for an advanced degree at the University of British Columbia, I agree that the Library shall make it freely available for reference and study. I further agree that permission for extensive copying of this thesis for scholarly purposes may be granted by the head of my department or by his or her representatives. It is understood that copying or publication of this thesis for financial gain shall not be allowed without my written permission.

Department of ___Electrical Engineering___

The University of British Columbia
Vancouver, Canada

Date ___Oct., 9, 1991___

Abstract

Y-branch optical modulators are potentially very useful in optical communications because of their non-interferometric nature, making them easier to fabricate and to control than other types of electro-optic switches. They can be used as digital optical switches, time division multiplexers, or in conjunction with a resonator as its electrode to form a high speed optical commutator switch. The main problem with Y-branch modulators to date is that they all have very small branch angles, e.g., less than 0.2°, and hence long electrodes, thereby increasing the device capacitance and reducing the switching speed. By studying a Y-branch optical modulator numerically and experimentally, our objective is to design a Y-branch modulator which has a short electrode and still offers high on/off ratios and high percentage guided power.

By using the effective index method along with the 2-D split-step finite difference beam propagation method, a z-cut titanium indiffused lithium niobate Y-branch modulator is simulated for a free space wavelength of 632.8 nm. The parameters varied in the simulations are: maximum refractive index change at the surface of the waveguide, electrode length, branch angle, and applied modulating voltage.

Based on the simulation results, a maximum refractive index change of 0.0042 and an electrode length of two-horn-length are used to provide good on/off ratios and percentage guided power while keeping the electrode short. Since the on/off ratios increase with branch angle while the percentage guided power decreases with branch angle, a range of angles between 1.0° and 1.5° are found to provide the preferred

operating characteristics.

Y-branch modulators with branch angles ranging from 0.5° to 3.0°, and with electrodes of two-horn-length as well as three-horn-length, are fabricated. The fabrication parameters are as specified in the simulations, e.g. waveguides are formed by diffusing 4 μm wide titanium strips at 1050°C for 6 hours. Previous fabrication problems such as dust accumulation and surface guiding are alleviated.

The devices are tested by launching polarized light from a helium neon laser into a polarization-maintaining fibre and then endfire coupling the light into the fundamental TM-like mode of the waveguides. The on/off ratios and percentage guided powers are measured for both devices with two-horn-length and three-horn-length electrodes. These measured results generally compare well with the theoretical values and the behaviours of all the Y-branch are as predicted. Using the 1.5° Y-branch with the two-horn-length electrode (300 μm) as an example, the experimental on/off ratio is 40:1 with a 66% guided power at 75 V while the theoretical values are 44:1 with 62% guided power.

We have demonstrated that a Y-branch electro-optic modulator with high on/off ratios and percentage guided power can be realized with short electrodes.

Table of Contents

List of Tables

List of Figures

Acknowledgements

Chapter I   Introduction

1.1   Importance of Y-branch Electro-optic Modulators

With the recent advances in optical communications, increasing research is required in the area of optical modulators. Although an optical signal can be directly modulated by the variation of injected current using a laser, external modulators such as electro-optic modulators are more attractive because they are capable of higher bit rate modulation and are needed for longer haul communication systems to maintain spectral purity. Furthermore, electro-optic modulators have potential uses as digital optical switches [1] as well as optical time division multiplexers [2]. Among the various types of electro-optic modulators, Y-branch optical modulators stand out as being very suitable for optical communication purposes because of their non-interferometric nature. They are relatively tolerant of variations in parameters such as wavelength and branch angle, and they also do not require a precise switching voltage or coupling length, unlike Mach-Zehnder type modulators and directional couplers. Y-branch electro-optic modulators therefore have the advantages of ease of fabrication and control when compared to other types of optical switches.

The basic layout of a Y-branch electro-optic modulator consists of a waveguide, leading into a Y-junction, and two waveguides branching out from the junction (see Figure 1.1 (a)). In its neutral state, without any voltage application, each arm guides an equal amount of light. Electrodes are usually placed near or at the junction, as in Figures 1.1 (b) and (c), so that the guided optical wave can be steered into one of the branch

arms as a result of the electro-optic effect during voltage application. In comparison with other types of electro-optic modulators, a Y-branch modulator is relatively simple in both structure and fabrication.
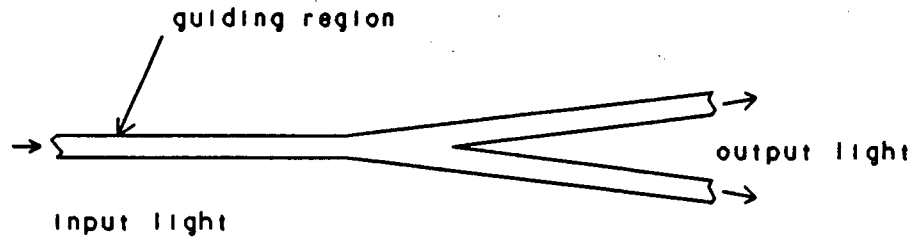
Figure 1.1 (a)   Y-branch waveguide
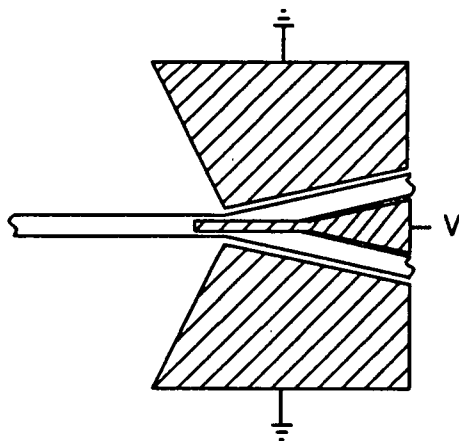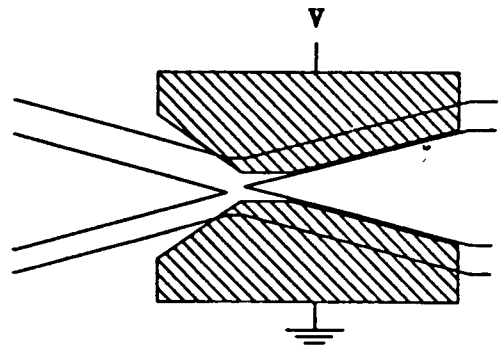
(b)   (c)

Figure 1.1 (b) & (c)   Common electrode layouts
                    - hatched areas are the electrodes [3,4]

An important consideration for optical modulators is the *on/off ratio*, which is defined as the ratio between the power guided in the *ON* and *OFF* states of a branch arm. Previous versions of the Y-branch electro-optic modulator having high on/off ratios and high percentage guided power all have either very small branch angles [3] (e.g., less than 0.2˚), or asymmetric branch arms [4] (see p.2). The problem with having small branch angles is that the long horn length, and hence the long device length and the difficulty associated with fabricating long devices, reduce the device yield on the substrate. Long devices also result in greater power loss due to attenuation, e.g., the attenuation factor for lithium niobate ($LiNbO_3$) titanium-indiffused waveguides is 1 dB/cm at $\lambda_o = 632.8nm$ [5]. Furthermore, a long horn length requires a long electrode, leading to increased capacitance and reduced switching speed. Y-junction asymmetries require tight fabrication tolerances, which is also undesirable. If a larger branch angle is used with a symmetric Y-branch layout, the modulator will be shorter reducing size, attenuation loss, and electrode capacitance. While devices with short electrodes have the above advantages, the drawback with a larger branch angle is the increased radiation loss, which leads to a lower percentage guided power at the output of the branch arms. A compromise between these factors is required for a good Y-branch modulator design.

1.2 Objective of Thesis

The goal of this work is to investigate and characterize the behaviour of a Y-branch electro-optic modulator fabricated on a z-cut $LiNbO_3$ substrate, where the waveguides are formed by titanium (Ti) indiffusion. We find, through numerical

simulations and experimental work, that better performance can be achieved than previously for a Y-branch configuration which has the combined properties of short electrode length, simple electrode shape, high on/off ratio and high percentage guided power at immediate voltages, e.g., 75 V.

A switching voltage of 75 V may seem too high for practicality in high speed switching due to the power requirements, especially when compared with a directional coupler type electro-optic switch which can switch at 18 V [6]. Our modulator, however, because of its short electrode, is capable of higher switching speeds and is not as sensitive to fabrication variations and should have higher yields due to its short length. More importantly, it can be used in conjunction with a resonator [7], serving as its electrode, to achieve switching speeds on the order of 10's of GHz with low power consumption. The power is kept low by using a resonator having a high Q factor. The layout of such an optical switch is shown in Figure 1.2, where a "*cul-de-sac*" resonator acts as the electrode for the Y-branch modulator. Such a device can act as a commutator switch forming the basis of a tree structure, whereby it can be used for time division multiplexing and demultiplexing.

An example of such a tree structure is shown in Figure 1.3, where each block is a commutator switch. Continuous light is divided into two pulse streams by the first switch operating at frequency *f*, then these two streams are divided into four pulse streams via switches operating at *f/2*, which are further divided into eight at *f/4*. These eight bit streams, which are time-division demultiplexed, can be then modulated by "killer switches", which may be travelling-wave electro-optic modulators. The coded

data are recombined via the commutators to give the output. The fan-out of such a structure is mainly limited by the size and power loss of the commutator switches. By designing a short Y-branch modulator which offers high on/off ratio and percentage guided power, it can used to realize this commutator switch.
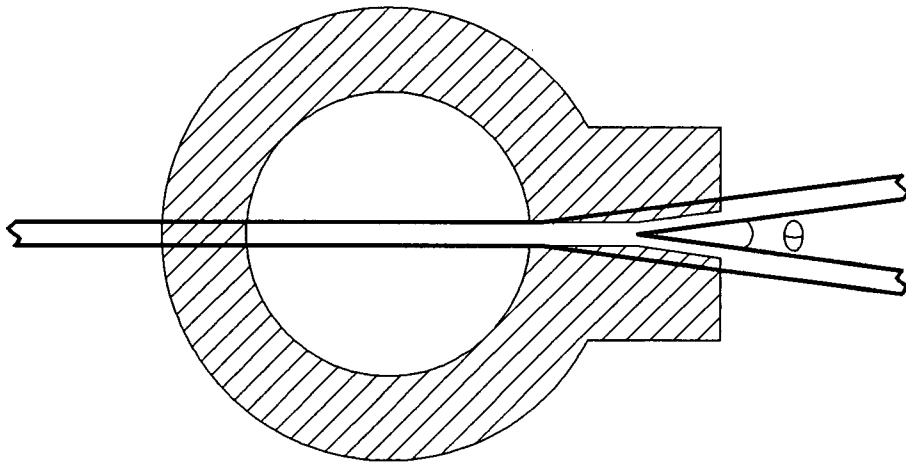
Figure 1.2 Y-branch waveguide with "cul-de-sac" resonator
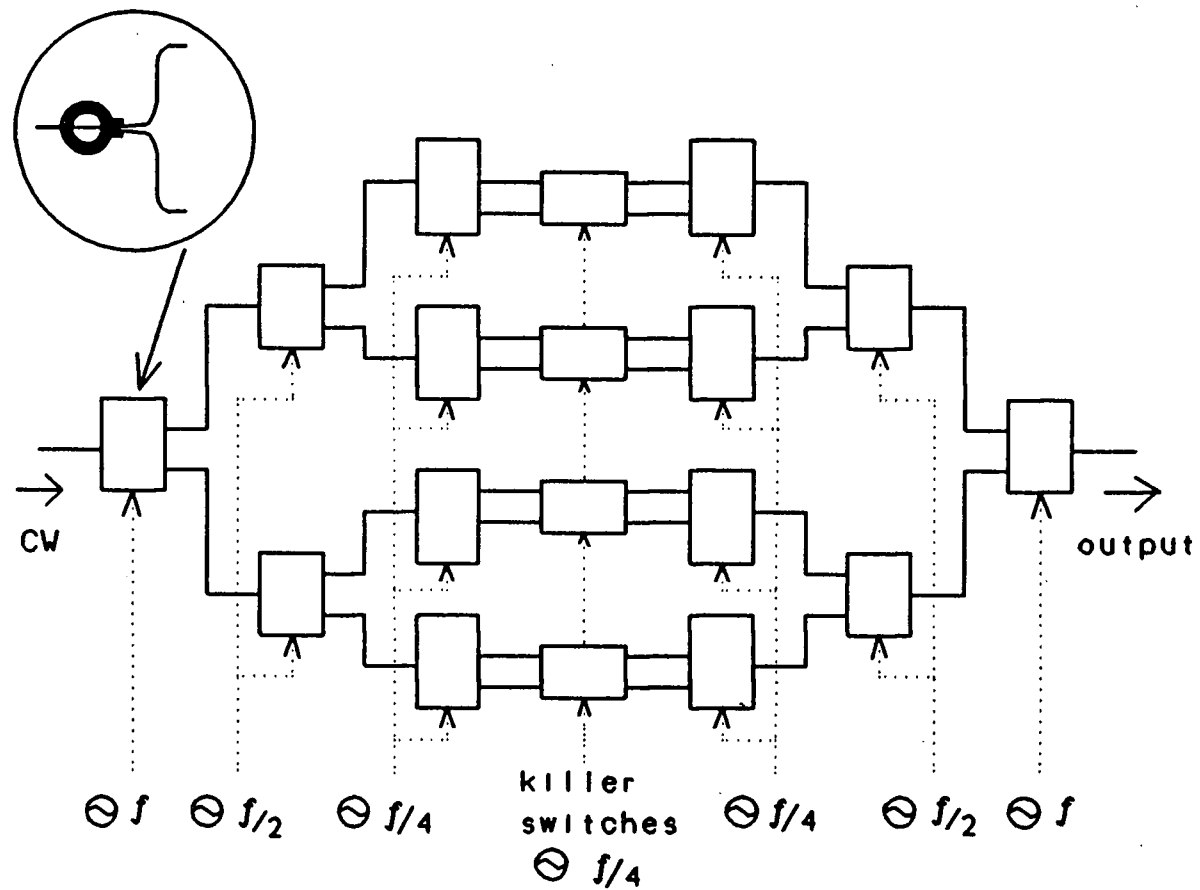
Figure 1.3 A tree structure using the Y-branch optical modulator as an optical commutator switch
Each block is a commutator switch as shown in Figure 1.2

CW

output

killer
switches

$\ominus f$ $\ominus f/2$ $\ominus f/4$ $\ominus f/4$ $\ominus f/2$ $\ominus f$

$\ominus f/4$

1.3 Organization of Thesis

In Chapter II, the basic operation of a Y-branch electro-optic modulator is discussed and some background about the recent advances in electro-optic modulators is provided.

The numerical modelling of the Y-branch optical modulator is described in chapter III, where the effective index method and the 2-D split-step finite difference beam propagation method are used to simulate the operation of the modulator.

Chapter IV provides the simulation results obtained from varying the following parameters: titanium thickness used for the indiffusion, electrode length, branch angle, and applied voltage. The performance of the modulator as a function of these parameters is described. A configuration for the Y-branch modulator, having high on/off ratio and percentage guided power, is found based on the simulation results.

In Chapter V, the layout of the masks used and the fabrication of the Y-branch optical modulator are described. The problems of dust accumulation and surface waveguiding are discussed and the remedies used are detailed.

Chapter VI provides the measured results of the fabricated Y-branch optical modulator. The test setup on the optics bench is described, followed by the methods used to calculate the on/off ratios and the percentage guided power. The measured results are then compared to the simulation results and the discrepancies are explained.

Recommendations for further work are given in chapter VII.

Finally, chapter VIII summarizes the work performed, and conclusions are given based on the theoretical and experimental results.

Chapter II   Background

2.1   Introduction

Electro-optic modulators operate by the linear electro-optic effect, exhibited by an electro-optic medium such as $LiNbO_3$. In the presence of an electric field, the electro-optic effect causes a change in the refractive index distribution in the guiding regions of the modulator. Such changes can be used to control the amount of light transmitted to the modulators output. Electro-optic modulators are usually of the Mach-Zehnder, the directional coupler, or the Y-branch type. In this chapter, the principle of the electro-optic effect will be briefly reviewed, followed by an overview of recent research in $Ti:LiNbO_3$ electro-optic modulators.

2.2   Electro-optic Effect

When an electric field is applied to a crystal exhibiting the linear electro-optic effect, such as $LiNbO_3$, a linear change in the refractive index occurs. This can be expressed by the relation

$$\Delta\left(\frac{1}{n^2}\right) = r\,E \qquad \left(\ or \qquad \Delta B_{ij} = r_{ijk}\,E_k\right) \tag{2.1}$$

where n is the refractive index, r is the electro-optic coefficient, E is the applied field, and B_{ij} is the relative dielectric impermeability. For $LiNbO_3$, the largest electro-optic coefficient is r_{33}. Therefore, when an electric field is applied parallel to the z-axis of the

crystal, a large change in the refractive index is seen by the z-polarized light. In LiNbO$_3$, the refractive index for the z-axis corresponds to the refractive index n_e of the extraordinary wave. At 633 nm, $r_{33} = 30.8 \times 10^{-12}$ m/V, and $n_e = 2.2$. In general, the Δn induced by an electric field is very small compared to n_e.

For z-cut LiNbO$_3$, the electrodes would have to overlap the waveguides (Figure 2.1 (a)) to use r_{33}, while for x- or y-cut LiNbO$_3$, the electrodes would have to be adjacent to the waveguides (Figure 2.1 (b)). By using z-cut LiNbO$_3$, a two-electrode configuration be used instead of one with three electrodes. Therefore, we have chosen to use z-cut LiNbO$_3$ for our work.
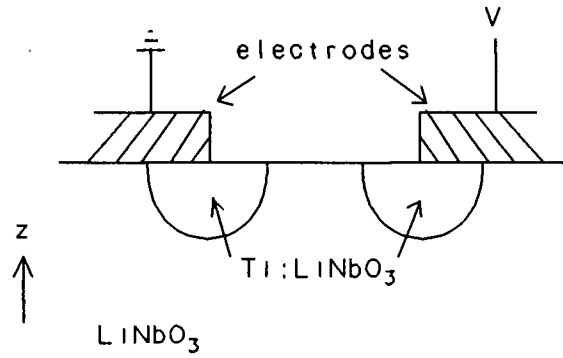
Figure 2.1 (a) Electrode placement for z-cut LiNbO$_3$
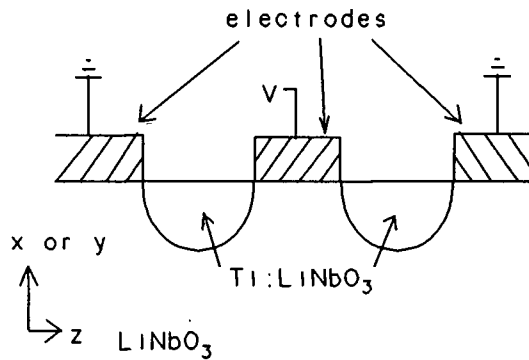
Figure 2.1 (b) Electrode placement for x- or y-cut LiNbO$_3$

2.3 Recent Research in Electro-optic Switches

For an electro-optic switch to be useful in optical communications, it should ideally have a high on/off ratio, high percentage guided power, and high switching speed. If the switch is to be manufactured reliably, then facility of fabrication is another factor to consider.

A commonly used figure of merit for integrated optics modulators is the *voltage-length* (V-L) product [8] (where *voltage* is the switching voltage, and *length* refers to the electrode length), with which the on/off ratio of a modulator generally increases. However, a large V-L product also increases the capacitance of the switch and hence reduces the switching speed for a given input power. One must therefore compromise between on/off ratio and switching speed.

Y-branch modulators operate on the principle that the refractive index of one branch arm increases while the index of the other arm decreases when a voltage is applied. As a result, we get one strongly guiding arm and one weakly guiding (or non-guiding) arm. The strongly guiding arm is the *ON* branch, while the weakly guiding arm is the *OFF* branch. The light is steered towards one arm or the other depending on the polarity of the applied field. The greater the electric field, the more strongly the light is steered into one of the branches.

Previous LiNbO$_3$ Y-branch devices had large V-L products due to very small branch angles, i.e. long electrodes. The reason for using small branch angles is to prevent excessive radiation loss, since it has been shown that radiation losses increase with branch angle [9]. However, we show that small branch angles (~ 1˚), with the

proper electrode configuration, result in only 1 dB radiation loss, which is equivalent to the loss incurred by a 1 cm long waveguide due to absorption [5].

The major drawback with having a small branch angle is the long horn length, and therefore the long electrode, required since the electrode has to modulate at least in the horn section, or longer in some cases. In Silberberg *et al.*'s four port digital modulator [4], a branch angle of 0.06° with an electrode length of 1.5 cm gives a 32:1 on/off ratio at 15 V. Similarly, a Y-branch modulator (fabricated using x-cut $LiNbO_3$) by Granestrand *et al.* [3] has a branch angle of 0.2° with an electrode length of 0.57 cm, its on/off ratio at 60 V is 25:1. A directional coupler type modulator generally gives a higher on/off ratio at a lower voltage, however, the fabrication tolerance is tighter due to the requirement of precise coupling length. For example, the directional coupler switch described in [6] claims to give an on/off ratio of 400:1 at 18 V using an electrode length of 1.9 cm. In all the above cases, except the directional coupler, small branch angles are used to ensure adiabatic power transfer in the taper region.

Perhaps a more meaningful figure of merit for a high speed modulator is the *power per unit bandwidth*, which lets the user know the amount of power required to drive the device at a particular frequency. In our work, we aim for a small power per unit bandwidth figure, a high on/off ratio, as well as ease of fabrication. One of our modulators, for example, has angle of 1.5° and an electrode of 300 μm giving an on/off ratio of 44:1 at 75 V. Due to its short electrode, the power per unit bandwidth $(P/\Delta f)$ is lower than other modulators known to date. Table I shows a comparison of our 1.5° device with other recent modulators. The power per unit bandwidth is calculated

according to Kaminow and Stulz's method [10] (see appendix A).

The good performance of our device is achieved by using a larger branch angle and a weakly guided wave. To overcome the excessive radiation loss associated with large branch angles, the modulating electrodes are placed so that more power can actually be guided during modulation than at 0 V. This is possible if a portion of the power radiated at 0 V can be captured into the *ON* branch when voltage is applied. The numerical simulations serve as a tool in this investigation.

Table I Performance Comparison

branch angle θ	electrode length (cm)	applied voltage (V)	on/off ratio	power/ bandwidth (W/GHz)
0.06° [4]	1.5	15	32:1	2.06
0.2° [3]	0.57	60	25:1	12.5
[6]	1.9	18	400:1	3.76
1.5°	0.03	75	44:1	1.03

Chapter III   Numerical Simulations

3.1   Device Layout and Model

The Y-branch electro-optic modulator to be simulated is shown in Figure 3.1.
Using z-cut LiNbO$_3$, the y-propagating waveguides are formed by titanium (Ti)
indiffusion. The width of the Ti strips prior to diffusion determines the number of
transverse modes supported by the waveguide. Strips 4 μm wide are assumed here in
order to guide the fundamental TM-like mode. The minimum thickness of the Ti
required is determined by that needed to ensure waveguiding. The desired Ti thickness
is found using the simulations. The diffusion process is assumed to occur at 1050˚C for
6 hours, giving a diffusion depth of 3 μm. An optical buffer layer of SiO$_2$ 2000Å thick
would be deposited on top of the entire substrate before placing the electrodes. Such a
buffer layer not only protects the diffused waveguides, but also prevents Joule losses of
the propagating TM mode due to interactions with the electrodes [11].   In the
simulations, the buffer layer is treated as a simple offset between the electrodes and the
substrate. Two electrodes are assumed to be placed symmetrically on either side of the
Y-branch. Various electrode lengths are used in the simulations. The branch angle θ is
also varied during the numerical simulations. A summary of the fabrication parameters
is provided in Table II.

The refractive index profile due to Ti-indiffusion is assumed to be Gaussian in
depth, since the theory of diffusion kinetics supports a Gaussian profile for long diffusion
times [12]. Minakata *et al.* [13,14] have measured and shown that Ti concentrations have

a Gaussian profile for diffusion times of several hours at temperatures between 950-1100°C. They have also produced calibration curves which show the relationships between the refractive index change Δn and the Ti concentrations, and have shown that Δn_e (for z-cut LiNbO$_3$) varies linearly with Ti concentration. The profile of the Ti concentration as a function of crystal depth was shown to be similar to a Gaussian function with the $1/e$ width equal to the diffusion depth, while the lateral profile of the Ti concentration was also shown to be Gaussian but with a much larger $1/e$ width.
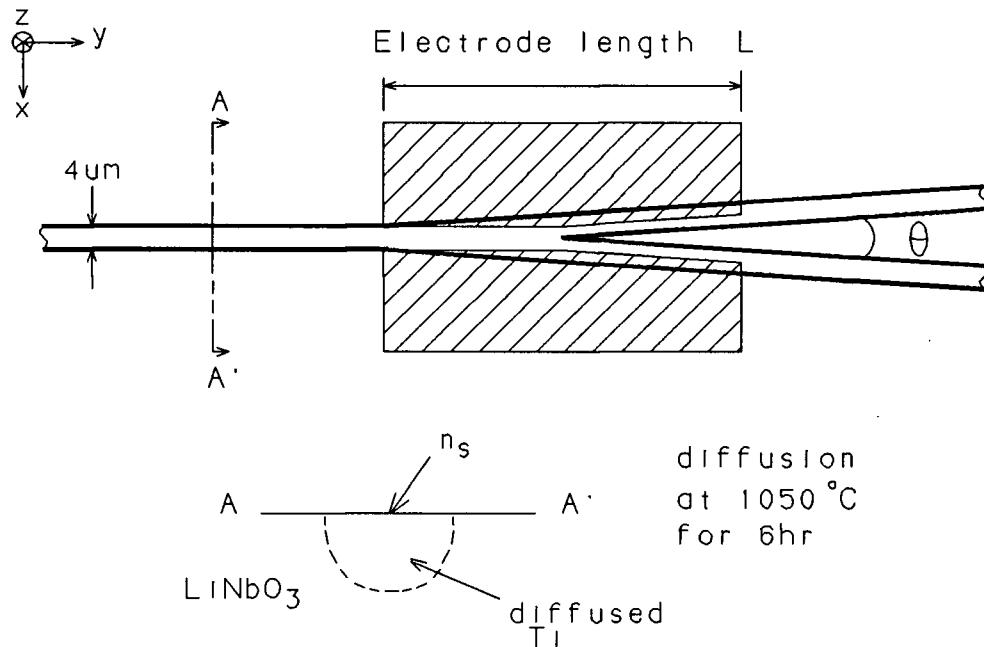
Figure 3.1 Layout of the Y-branch optical modulator

For the sake of simplicity, we have adopted the model from Hocker and Burns [15] for the refractive index profile, where the refractive index change is a Gaussian function depthwise and an error function widthwise. Although this model differs from Minakata et al.'s measurement for the lateral profile, the profiles are similar and the one we have chosen has been widely used without introducing gross errors. The refractive index profile $n(x,z)$ for the simulated modulator is then [15]:

$$n^2(x,z) = n_b^2 + (n_s^2 - n_b^2)f(\frac{z}{D})g(\frac{2x}{W})$$

(3.1 a)

where

$$f(\frac{z}{D}) = \exp(-\frac{z^2}{D^2})$$

(3.1 b)

and

$$g(\frac{2x}{W}) = 1/2\left(erf\left[\frac{W}{2D}\left(1 + \frac{2x}{W}\right)\right] + erf\left[\frac{W}{2D}\left(1 - \frac{2x}{W}\right)\right]\right)$$

(3.1 c)

D is the diffusion depth which is function of diffusion temperature and time ($D = 2(Đt)^{1/2}$, t is time, and $Đ$, the diffusion temperature coefficient, is 1.06×10^{-12} cm^2/s at 1050°C for a congruent composition of 48.6 mol % LiO$_2$ [16]), W is the width of the Ti strip prior to diffusion, n_b is the bulk refractive index for z-cut LiNbO$_3$ at $\lambda_o = 632.8$ nm, and n_s is the maximum refractive index at the surface due to the Ti indiffusion.

Table II Fabrication Parameters

Titanium thickness	variable parameter
bulk refractive index n_b	2.2
maximum refractive index n_s	depends on Ti thickness
diffusion depth D	3 μm
diffusion temperature	1050°C
diffusion time	6 hrs
SiO_2 buffer layer thickness	2000Å
Aluminum thickness for electrodes	4000Å
waveguide pattern width W	4 μm
electrode gap at input	4 μm
electrode gap at output	depends on electrode length

3.2 Simulation Methods

Although many numerical modelling methods exist which can simulate integrated optic devices, e.g., the finite element and the mode-matching methods [17], the beam propagation method (BPM) is chosen due to its speed and simplicity. It is a commonly used method for successively calculating the electromagnetic field along the direction of propagation in a stepwise fashion. Propagation modes and radiation modes alike can be treated simultaneously by the BPM. Although the BPM is not based on solving the full Maxwell's equations but rather the scalar Helmholtz equation, it has been shown to be sufficiently accurate as long as the refractive index varies gradually along the direction of propagation [17]. The assumptions necessary for the validity of the BPM include negligible reflections, paraxiality of the fields, and low contrast of dielectric structure.

The Y-branch electro-optic modulator satisfies all these constraints if the branch angle is less than 5° and the propagating step length in the horn section is small. The refractive index change for the modulator is gradual depthwise and widthwise since they are Gaussian and error functions respectively. The only sudden change in the refractive index occurs during voltage application at the boundaries of the electrodes.

The BPM can be used for a three dimensional simulation or a two dimensional simulation. The 2-D method is chosen for our work due to its increased speed and comparable accuracy [18]. When using the 2-D method the 3-D refractive index profile needs to be reduced to 2-D, which is commonly performed by using the effective index method [15] developed by Hocker and Burns.

3.2.1   Effective-Index Method

In the effective index method (EIM), an effective index of refraction n_{eff} can be defined for each mode in a waveguide using the phase constant β:

$$n_{eff} = \frac{\beta}{k_o}$$

(3.2)

where k_o is the free-space phase constant ($k_o = 2\pi/\lambda_o$), and the limits on n_{eff} are

$$n_b < n_{eff} < n_s$$

(3.3)

For our Y-branch modulator, the EIM can be used to reduce the profile defined by $n(x,z)$ in equation 3.1 (a) to an effective index $n_{eff}(x)$, a function of x only. At each

coordinate x, the waveguide is treated as a planar waveguide with an index profile which varies only depthwise. An effective index $n_{eff}(x)$ for this planar waveguide can be found if it supports a propagating wave. When the Y-branch modulator is in its neutral state without voltage application, $n_{eff}(x)$ is computable for all regions of x where the waveguide lies, and for regions in which $n_{eff}(x)$ is not computable, it is approximated by n_b. Figure 3.2 shows the refractive index profile $n(x,z)$ and Figure 3.3 illustrates the calculated effective index $n_{eff}(x)$ using the method described in reference [19].
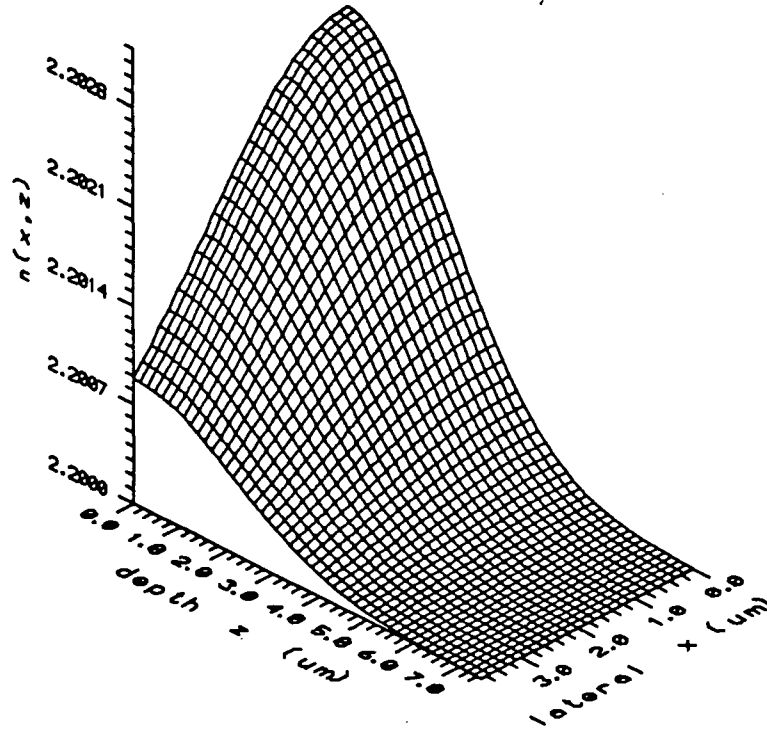
Figure 3.2   2-D refractive index profile n(x,z)
- for 0 μm < x < 4 μm
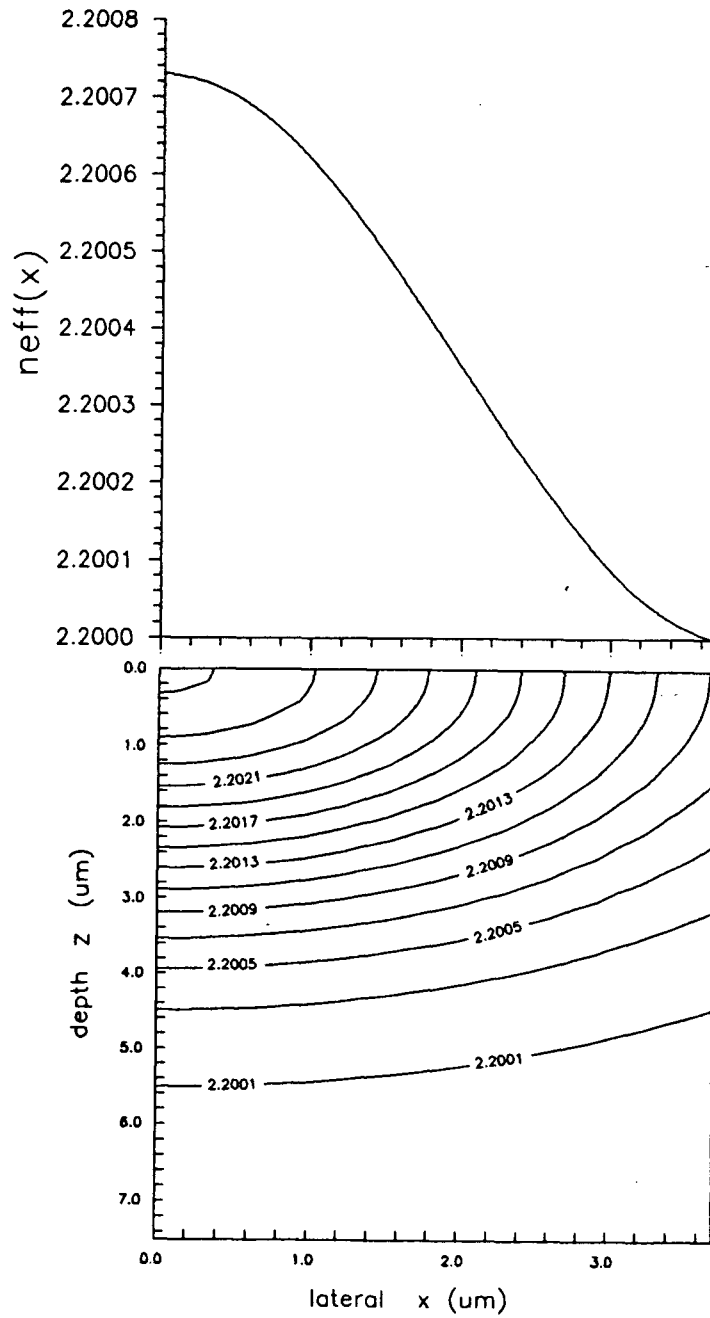
Figure 3.3 1-D effective index profile $n_{eff}(x)$ and the corresponding 2-D
topographic view of $n(x,z)$

3.2.2 2-D Finite Difference Beam Propagation Method

As mentioned earlier, the simulations are performed by first applying the EIM and then by using the 2-D BPM to calculate the optical field. Conventional BPM requires the use of the standard Fast Fourier Transform (FFT) twice for every propagating step. Therefore, a faster version of the BPM is employed, called the split-operator Finite Difference BPM (FDBPM) developed by D. Yevick [20]. Similar to the BPM, the FDBPM is also based on the Fresnel approximation of the scalar Helmholtz equation. The difference lies in using the split-operator finite-difference scheme to model the free-space propagation step. This method involves the solving of a tridiagonal matrix rather than using the FFT. The evolution of the electric field for a single polarization of a monochromatic optical wave for a 2-D problem is given by [20]:

$$
\mathscr{E}(x, y + \Delta y) = \left[D_x \, e^{-\frac{ik_o}{2n_b} \int_y^{y+\Delta y} (n_{\text{eff}}^2(x, y') - n_o^2) dy'} \, D_x \right] e^{-ik_o n_b \Delta y} \mathscr{E}(x, y) + O(\Delta y)^3 \tag{3.4a}
$$

where

$$
D_x \equiv \frac{1 + \dfrac{-i\Delta y}{8 k_o n_b} \dfrac{\partial^2}{\partial x^2}}{1 - \dfrac{-i\Delta y}{8 k_o n_b} \dfrac{\partial^2}{\partial x^2}} \tag{3.4b}
$$

As in the standard BPM, the physical model of the FDBPM is as follows: light propagates through free-space for distance $\Delta y/2$, then through a lens with refractive index distribution $n_{\text{eff}}(x)$, then again through free-space for distance $\Delta y/2$. According to equations 3.4 (a) and (b), the free-space propagation term is represented by D_x, while the

lens term is represented by the exponential term with the integral. The entire process can be viewed as propagating a light beam through a periodic array of thin lenses, refocussing the light beam during each step.

In our simulation, a 100 μm wide computation window with 1000 transverse grid points is used. Since the boundary condition of zero electric field at the computational window edge is required when using the BPM, an absorber is placed 15 μm on either side of the window edges to prevent high frequency numerical instabilities [21]. The absorber is obtained by multiplying the electric field by the function:

$$
absorber\ (x) \ = \ \begin{cases} 1, & |x| \leq 35\mu m \\ \dfrac{1}{2}\left(1 + \cos\left(\dfrac{\pi\left(|x| - 35\right)}{15}\right)\right), & 35\mu m < |x| < 50\mu m \\ 0, & |x| = 50\mu m \end{cases}
\tag{3.5}
$$

3.2.3 Effective Index Calculation During Voltage Application

When simulating the effect of voltage application to the coplanar electrodes, conformal mapping [22] is used to evaluate the electric fields in the x and z directions of the crystal, E_x and E_z respectively, where

$$
E_x \ = \ \frac{V}{\pi} \ \frac{\cos\left(\dfrac{1}{2}\tan^{-1}\left(\dfrac{2xz\sqrt{\epsilon_x/\epsilon_z}}{h_{gap}^2 - x^2 + z^2\,\epsilon_x/\epsilon_z}\right)\right)}{\sqrt[4]{4x^2z^2\,\epsilon_x/\epsilon_z + \left(h_{gap}^2 - x^2 + z^2\,\epsilon_x/\epsilon_z\right)^2}}
\tag{3.6 a}
$$

$$E_z = \frac{V}{\pi} \frac{\sin\left(\frac{1}{2}\tan^{-1}\left(\frac{2xz\sqrt{\epsilon_x/\epsilon_z}}{h_{gap}^2 - x^2 + z^2\,\epsilon_x/\epsilon_z}\right)\right)}{\sqrt[4]{4x^2z^2\,\epsilon_x/\epsilon_z + \left(h_{gap}^2 - x^2 + z^2\,\epsilon_x/\epsilon_z\right)^2}} \qquad (3.6\,b)$$

V is the applied voltage, ϵ_x and ϵ_z are the dielectric constants for LiNbO$_3$ in the x and z directions and are 43 and 28 respectively, and h_{gap} is half the gap distance between the two electrodes.

When a voltage is applied to the electrodes, the electric fields modify the refractive index profile through the electro-optic effect, and a modulated refractive index profile $n(x,z) + \Delta n(x,z)$, where $n(x,z)$ is from equation (3.1), is thus obtained. $n_{eff}(x)$ can increase or decrease due to this change giving a new value here called the modulated effective index $n'_{eff}(x)$.

One problem which arises is when a voltage is applied beyond that for which $n'_{eff}(x)$ is calculable. Usually as long as the actual refractive index distribution decreases monotonically with depth into the substrate, one replaces $n_{eff}(x)$ or $n'_{eff}(x)$ with n_b when a value for the effective index cannot be obtained. However, with a field applied, a large enough change in the index distribution can reduce the index so much that such an approximation is no longer valid; here we call these regions "non-guiding regions". For example, a large field might be applied causing the index to increase substantially with depth, in which case $n'_{eff}(x)$ should be substantially less than n_b. $\Delta n_{eff}(x)$ is here defined to be the difference in effective index between the modulated and the unmodulated values, i.e., $n'_{eff}(x) = n_{eff}(x) + \Delta n_{eff}$. We show that this is correct under the weakly guiding approximation when $\Delta n_{eff}(x)$ is negative as well as when it is positive. Hence a value

may be obtained for $n'_{eff}(x)$ in regions where strictly speaking it cannot be calculated due to the nature of the actual refractive index distribution.

3.2.3.1 Effective Index Calculation in Non-guiding Regions

The $n_{eff}(x)$ in non-guiding regions can be calculated by using a second index distribution for which a $n_{eff}(x)$ value may be obtained, and then perturbing it to a third distribution for which a value $n'_{eff}(x)$ may also be obtained (where $n'_{eff}(x) > n_{eff}(x)$), the perturbation being equal but opposite to that of the second distribution from the original distribution. This method can be employed conveniently for our simulation since the electrodes for our Y-branch modulator are coplanar, and therefore the electric fields (and hence the $\Delta n(x,z)$) are equal but opposite in polarity about the centre $x = 0$. By calculating $n'_{eff}(x)$ for the side with a positive change in the refractive index, e.g. $+\Delta n(x_1,z)$, (which is computable using the EIM), a positive value $\Delta n'_{eff}(x) = n'_{eff}(x) - n_{eff}(x)$ can be obtained. The $n'_{eff}(x)$ value for the non-guiding side due to an equal but opposite change in the index, e.g., $-\Delta n(x_1,z)$, can be shown to be equal to $n_{eff}(x) - \Delta n'_{eff}(x)$.

To do this we begin by assuming that the optical field $\mathscr{E}_z(x,z)$ is separable, i.e., $\mathscr{E}_z(x,z) = A\psi(x)\phi(z)$, where $\psi(x)$ and $\phi(z)$ are normalized functions and A is a scaling factor. Hence, at any coordinate (x_1,y_1), the optical field $\mathscr{E}_z(x_1,z) = C\phi(z)$ where $C = A\psi(x_1)$. Although an approximation, this is reasonable and commonly used for diffused strip waveguides, e.g., the optical field was found in Keil and Auracher [23] to be approximately Gaussian in width and Hermite-Gaussian in depth.

Since the expression for the propagation constant β is known [24], and using

$n_{eff} = \beta/k_o$, $n_{eff}(x)$ can be obtained from:

$$n^2_{eff}(x) = \frac{\int_{-\infty}^{\infty} \left[n^2(x,z) \phi \phi^* - (\nabla\phi) \cdot (\nabla\phi^*) \right] dz}{\int_{-\infty}^{\infty} \phi \phi^* \, dz} \qquad (3.7)$$

given $\phi(z)$ and $n(x,z)$. However, even if $\phi(z)$ is not known exactly, $n_{eff}(x)$ can still be calculated from (3.7) by using a good approximation of $\phi(z)$ because β^2 is stationary to the first order with respect to $\phi(z)$.

Now, let the refractive index be perturbed such that $n(x,z)$ is replaced by $n(x,z) + \Delta n(x,z)$ and assuming $\phi(z)$ is unchanged, (3.7) can be solved giving

$$n'^2_{eff} = n^2_{eff} + 2n_{eff} \Delta n_{eff} + (\Delta n_{eff})^2 \qquad (3.8)$$

where $n = n(x,z)$ and

$$2 \Delta n_{eff} \, n_{eff} = \int_{-\infty}^{\infty} 2n \Delta n \phi \phi^* \, dz \qquad (3.9)$$

or

$$\Delta n_{eff} = \frac{1}{n_{eff}} \int_{-\infty}^{\infty} n \Delta n \phi \phi^* \, dz \qquad . \qquad (3.10)$$

From (3.10), the sign of Δn_{eff} is clearly determined by the function $\Delta n(x,z)$, i.e., if $\Delta n(x,z)$ gives a value Δn_{eff}, then $-\Delta n(x,z)$ would give $-\Delta n_{eff}$. Therefore, if $n'_{eff}(x) = n_{eff}(x) + \Delta n_{eff}(x)$ for a particular change in the refractive index, then $n'_{eff}(x) = n_{eff}(x) - \Delta n_{eff}(x)$ for an equal but opposite change in the refractive index.

To better illustrate the application of the above method in our Y-branch modulator simulation, Figures 3.4 and 3.5 show the $n_{eff}(x)$ profile for no voltage application, and the $n'_{eff}(x)$ profile with 50 V applied respectively. In Figure 3.4, the profile is symmetric about $x = 0$ for all y, i.e. $n_{eff}(x) = n_{eff}(-x)$. With voltage applied, (as in Figure 3.5),

$n'_{eff}(x)$ is computed directly from the EIM for the strongly guiding arm $(n'_{eff}(x) > n_{eff}(x))$, whereas the $n'_{eff}(x)$ for the weakly guiding arm $(n'_{eff}(x) < n_{eff}(x))$ is calculated using the described method. In Figure 3.5, $n_{eff}'(x_1) = n_{eff}(x_1) + \Delta n_{eff}(x_1)$ giving $\Delta n_{eff}(x_1) = n'_{eff}(x_1) - n_{eff}(x_1)$, where $n'_{eff}(x_1)$ can be obtained from the EIM and $n_{eff}(x_1)$ is calculated for 0 V applied, i.e., the case depicted in Figure 3.4. Then at $x = -x_1$, $n'_{eff}(-x_1) = n_{eff}(x_1) - \Delta n_{eff}(x_1)$ since $n_{eff}(x_1) = n_{eff}(-x_1)$. The unmodulated profile is also shown in Figure 3.5 for reference, (dashed line).

3.3   Input and Output

The input to the Y-branch modulator is the fundamental TM-like mode with unit power, here called the eigenfunction $U_o(x)$. $U_o(x)$ is the lowest order mode which can propagate through the straight unperturbed waveguide with no loss in power. To calculate the eigenfunction $U_o(x)$, a commonly used procedure described in reference [25] is employed. This procedure works well with any BPM and is described briefly here.

Firstly, an arbitrary electric field distribution $E(x,0)$, such as a Gaussian profile with a beam waist of 4 μm, is allowed to propagate down the straight unperturbed waveguide for a length Y by repeatedly applying equation 3.4. Then the propagation constants of the modes comprising $E(x,0)$ can be determined by computing the correlation function

$$P(y) = \int E^*(x,0) E(x,y) \, dy \qquad (3.11)$$

If $P(y)$ is multiplied by a Hanning window and then Fourier transformed, the propagation
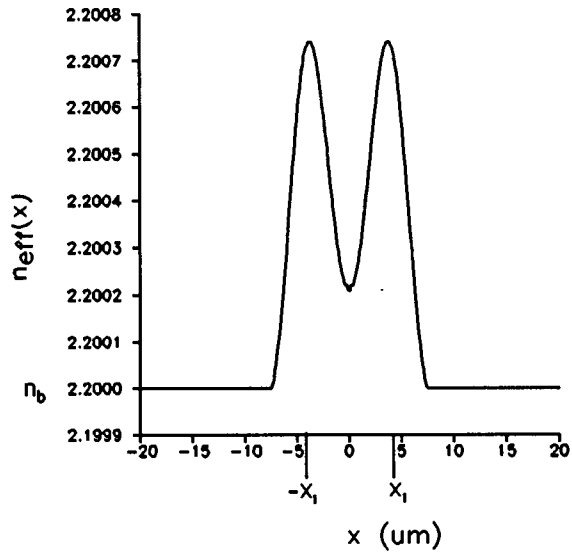
Figure 3.4 Unmodulated effective index $n_{eff}(x)$
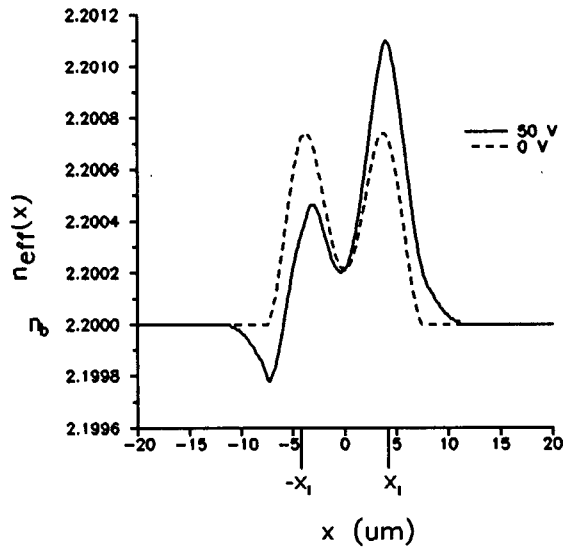
Figure 3.5 Modulated effective index $n'_{eff}(x)$ during voltage application

constant β_i of each mode for the profile $E(x,0)$ can be found by using a line-fitting procedure [26] and by taking into account that $n_b k_o < \beta < n_s k_o$. $U_i(x)$ can subsequently be evaluated by integrating $E(x,y)$ with the corresponding β_i as follows [25]:

$$U_i(x) = \frac{1}{Y} \int_0^Y E(x,y) w(y) e^{i\beta_i y} dy$$

(3.12)

where $w(y)$ is an appropriate window function such as a Hanning window. Therefore,

$$U_o(x) = \frac{1}{Y} \int_0^Y E(x,y) w(y) e^{i\beta_o y} dy$$

(3.13)

for our case, $Y = 2048$ μm for 2^{11} steps at 1 μm intervals.

Once the $U_o(x)$ is determined for the particular maximum refractive index n_s being used, the Y-branch modulator can be excited with the modal eigenfunction and its propagation behaviour can then be examined.

The output power of the modulator at a distance y can be evaluated by taking the inner product of the propagating field with the eigenfunction $U_o(x)$. In the straight section of the Y-branch (before the horn), the power is

$$P(y) = \left| \int E(x,y) U_o^*(x) \, dx \right|^2$$

(3.14)

For the power output at the branching section, the eigenfunction $U_o(x)$ would have to be shifted in (3.14) to overlap the two branch arms properly. In the simulations, we have decided to compute the power output when the two arms are 40 μm apart centre to centre so that the optical fields no longer interact with each other. The power is then

$$P(y) = \left| \int E(x,y) U_o^*(x-20) \, dx \right|^2 + \left| \int E(x,y) U_o^*(x+20) \, dx \right|^2$$

(3.15)

The on/off ratio of the modulator with voltage application is taken as the ratio of the power in the strongly guiding arm to the power in the barely guiding arm.

3.4   Simulation Procedure

To prevent sudden changes in the refractive index profile and to minimize reflections when the Y-branch is spreading out, the Y-junction and the branching arms of the modulator are made to step out at 0.1 μm (which is equal to the step size possible in a electron-beam fabricated mask). The longitudinal step length Δy varies for each branch angle so that the number of steps required to reach the 40 μm separation point can be kept approximately constant for all the branch angles. The step length and its corresponding angle are shown in Table III. The horn length is divided into 20 sections, and each of those consists of 20-30 sections of Δy.

Table III   Step length Δy

branch angle θ	step length Δy (μm)
0.5°	1.0
1.0°	0.5
1.5°	0.3
2.0°	0.19
2.5°	0.23
3.0°	0.19

The entire simulation procedure can be summarized as follows:

1. Calculate the eigenfunction $U_o(x)$.

2. Evaluate the effective index $n_{eff}(x)$.

3. Evaluate the modulated effective index $n'_{eff}(x)$ when a voltage is applied.

4. Propagate $U_o(x)$ through the Y-branch modulator.

5. Calculate the power guided and the on/off ratio.

The complete simulation program is written in Pascal and Turbo Pascal version 4.01 by Borland is used to compile and run the program. Running on a 33 MHz IBM-386 compatible machine with a math co-processor, approximately 1.5 hours are required for each simulation on average if the eigenfunction $U_o(x)$ is predetermined.

Chapter IV Simulation Results

4.1 n_s - Maximum Refractive Index at the Surface

The first investigation performed using the numerical simulations was to determine a value for n_s (giving the required Ti thickness) for the Y-branch waveguides. A value for n_s resulting in weakly guided light which can be easily steered by applying a voltage is desirable. If the waveguides are too strongly guiding, then the voltage-induced refractive index changes will not be sufficient to make the necessary difference to the index profile. However, if n_s is too small, no waveguide is created.

We begin by using n_s = 2.205, i.e., the maximum refractive index change $\Delta n_s = n_s - n_b = 0.0050$, which corresponds to approximately 0.667% Ti concentration by weight at the surface for z-cut LiNbO$_3$ at λ = 632.8 nm [27]. The eigenfunction $U_o(x)$ is found first, then it is used to excite a 0.5° Y-branch modulator with a two-horn-length electrode at 80 V. The on/off ratio evaluated is 4.6:1 and the power guided is 80% (100% power guided being for a straight waveguide). Since the on/off ratio is very low and the power guided is high, the waveguides are too strongly guiding for the intended purpose.

The next Δn_s we attempt uses Δn_s = 0.0042, which corresponds to 0.565% Ti[1]. The simulation results showed an improvement with a branch angle θ = 0.5°. The

---

[1] This is equivalent to indiffusing a layer of Ti approximately 480Å thick (see appendix B for calculation), which past fabrication experience at UBC solid state laboratory has shown will produce waveguides at λ_o = 632.8 nm.

on/off ratio at 80 V is 10:1, and the power guided is approximately 70%.

Then we set $\Delta n_s = 0.0035$, which corresponds to 0.467% Ti. With this low Δn_s, the guide is found to be incapable of guiding the fundamental TM-like mode.

Our results showed that for a 6 hour diffusion at 1050°C, $\Delta n_s = 0.0035$ is too low to produce waveguides, $\Delta n_s = 0.0050$ is too high for the intended application, whereas $\Delta n_s = 0.0042$ could both be useful and was consistent with currently used fabrication procedures.

Figure 4.1 shows the on/off ratios at various voltages obtained from the various Δn_s values. With $\Delta n_s = 0.0042$, a modulator with a 2° branch angle at 80 V has an on/off ratio of 84:1 with about 50% of the power guided, while with $\Delta n_s = 0.0050$ the on/off ratio under the same conditions is 43:1 with 53% of the power guided. Since $\Delta n_s = 0.0042$ provides much higher on/off ratios while losing only a few percent of guided power, it is selected for our subsequent simulations. It should be pointed out that a value other than $\Delta n_s = 0.0042$ could lead to improved performance. However, as mentioned, this value is very realistic due to its correspondence to a known fabrication procedure. Figure 4.2 shows the optical power of the eigenfunction $U_o(x)$ which corresponds to $\Delta n_s = 0.0042$, the spot size (defined as the full width at half the maximum power) is 4 μm.

4.2 Electrode Length

As mentioned previously, the electrodes should be as short as possible to minimize capacitance. However, poor modulation and low on/off ratio result if the electrodes are too short. This is because there is not enough change in the refractive index to steer the
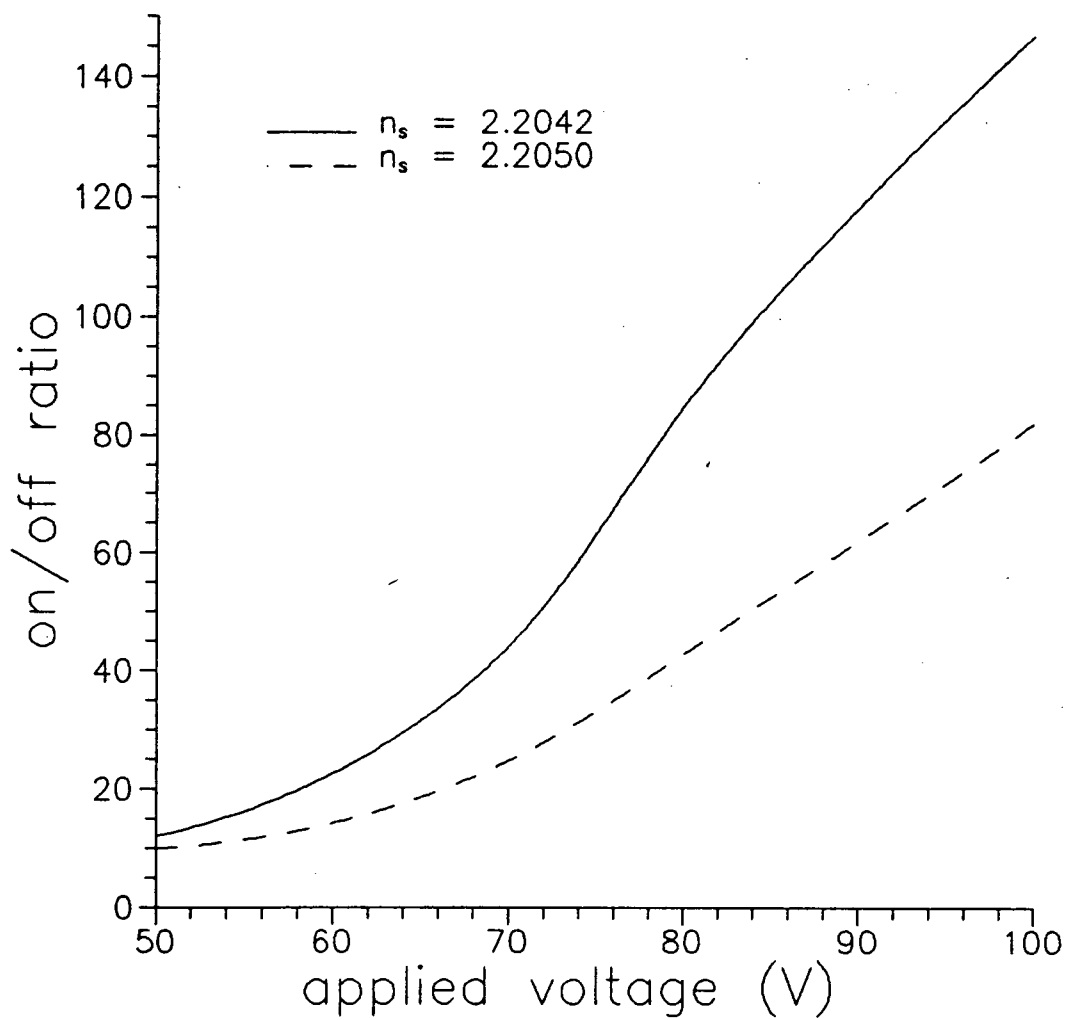
Figure 4.1 On/off ratios for a 2.0° branch with a two-horn-length electrode at various voltages for $\Delta n_s = 0.0050$ and $\Delta n_s = 0.0042$
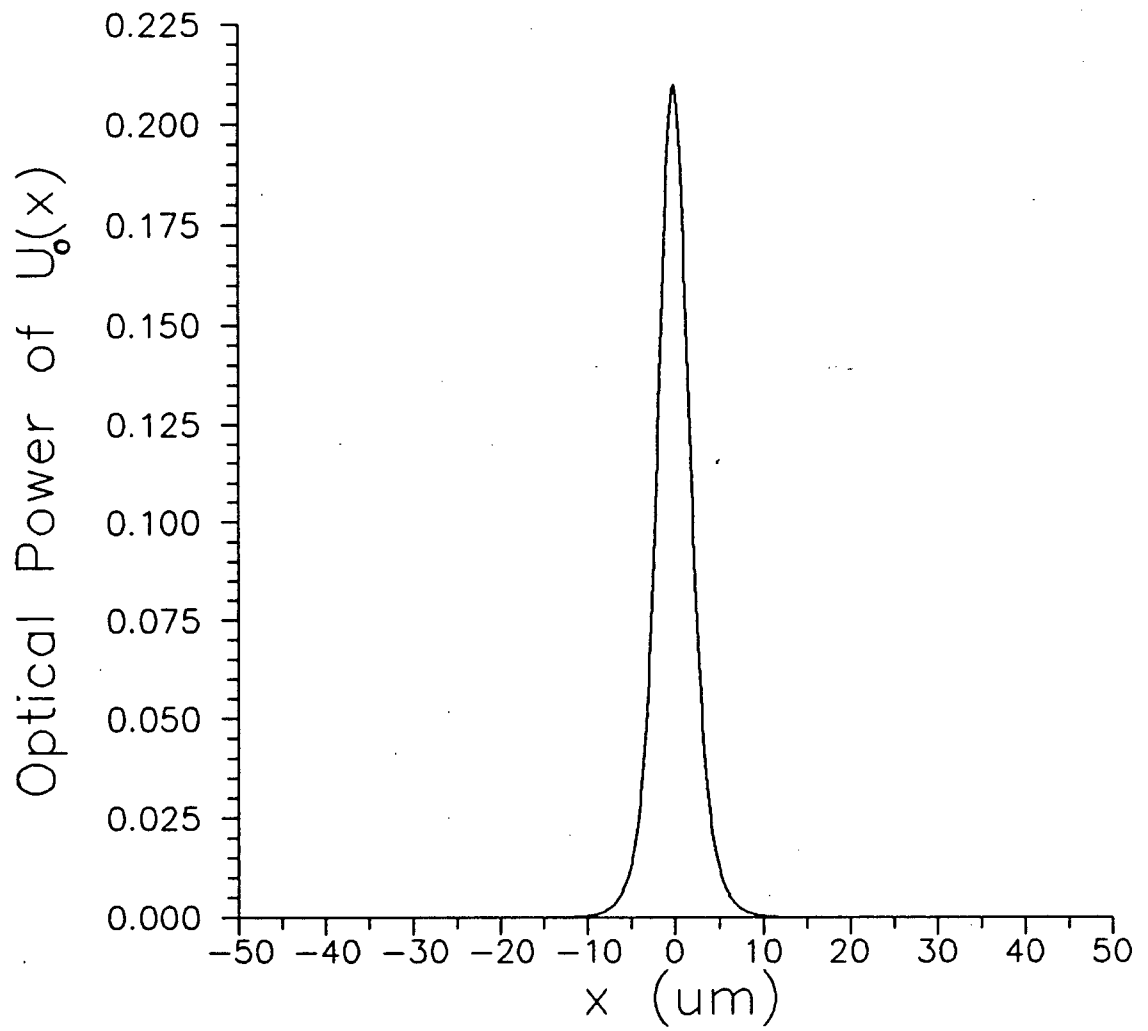
Figure 4.2 Eigenfunction $U_o(x)$ for $\Delta n_s = 0.0042$

light into the *ON* branch. To investigate the effect of electrode length on the performance of the modulator, a 2° Y-branch is simulated with three different electrode lengths: one-horn-length, two-horn-length, and three-horn-length long electrodes. All the electrodes originate from the same location, i.e., at the beginning of the horn.

The one-horn-length electrode fails to cause substantial modulation of the optical fields in the two arms. The on/off ratio is very low because of the small amount of steering. Due to the poor results obtained we abandoned the single-horn-length electrode simulations.

Comparing the results for the two-horn-length electrode with those for the three-horn-length electrode, the two-horn-length electrode is found to give higher on/off ratios (see Figure 4.3). This may seem surprising at first because longer electrode lengths are generally associated with higher on/off ratios. The fact that the on/off ratios from the three-horn-length electrode are actually lower than those from the shorter electrode may indicate cross coupling effects. Although we are dealing with large branch angles for Y-branch modulation, the angles are still fairly small, i.e., the two branch arms are still nearly parallel, such that some coupling will result. In any case, the three-horn-length electrode shows, in no instance, any notable improvement in performance over the two-horn-length electrode but obviously increases the capacitance of the modulator. Since one of the criteria in electrode selection is to minimize capacitance a two-horn-length electrode is chosen.
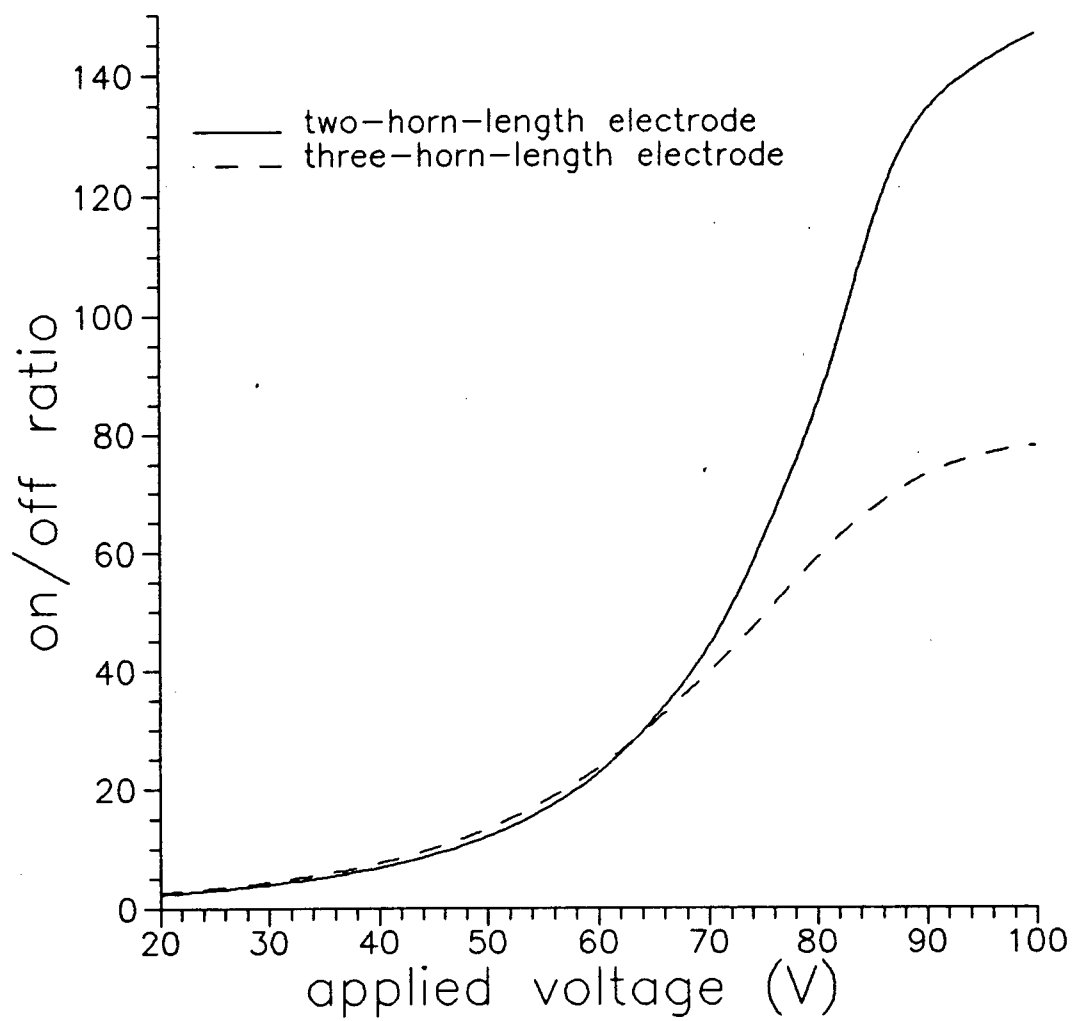
Figure 4.3 On/off ratios for a 2° Y-branch at two different electrode lengths

4.3 Effects of Branch Angle

To investigate the effect branch angle θ has on the performance of the modulator, devices having branch angles of 0.5°, 1.0°, 1.5°, 2.0°, 2.5°, 3.0° are simulated. The Δn_s is 0.0042 and the electrode length used is two-horn-length long. The theoretical amount of guided power for the various θ with 0 V, 50 V, and 75 V applied is shown in Figure 4.4. The on/off ratios for 50 V and 75 V are shown in Figure 4.5. The general trend is that the guided power decreases with increasing branch angle (above 1°), while the on/off ratios increase with increasing branch angle [28]. The guided power is expected to decrease with increasing angle θ because of the increased radiation loss, regardless of voltage application. When a voltage is applied, however, light is channelled into the *ON* branch but not into the other branch. As the branch angle increases, the greater this discrepancy becomes and the higher the on/off ratios can be obtained. Referring to Figure 4.6, the operation of the modulator can be classified into three regions according to angle θ. Region I is for θ less than 0.8°; region II is for those with θ between 0.8° and 2.0°; region III is for θ greater than 2.0°.

4.3.1 Region I

In this region, the on/off ratios are low while the guided power is high. The high guided power is due to the shallow branch angle, i.e., low radiation loss. With no voltage applied, the percentage guided power is over 90%. With voltage application, however, the optical power in the *ON* branch increases moderately but is greatly

36
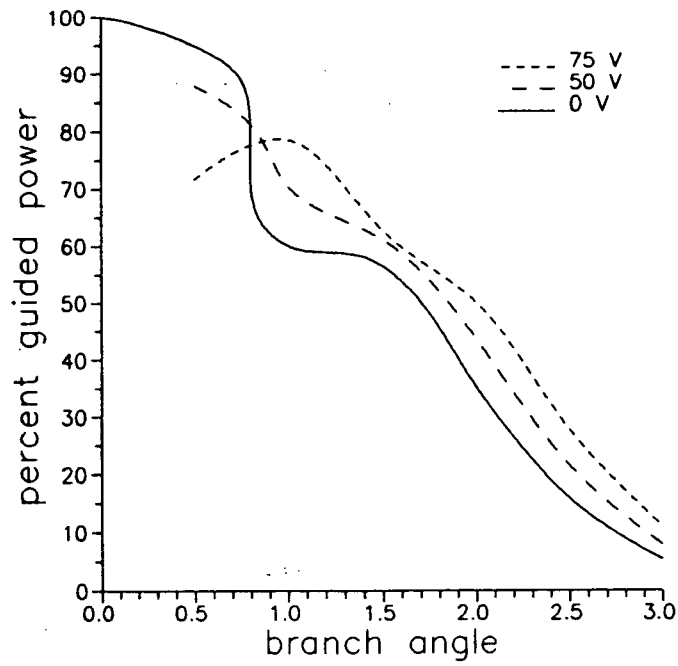
Figure 4.4 Percentage guided power vs. branch angle θ
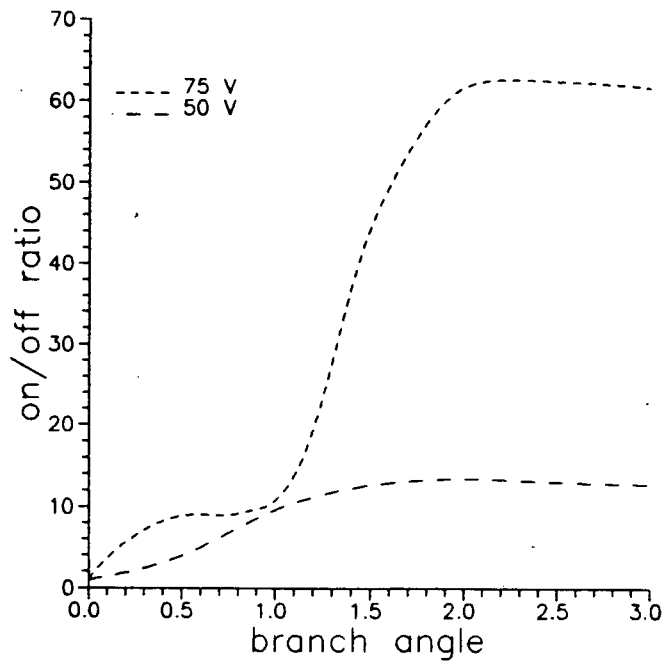
Figure 4.5 On/off ratio vs. branch angle θ
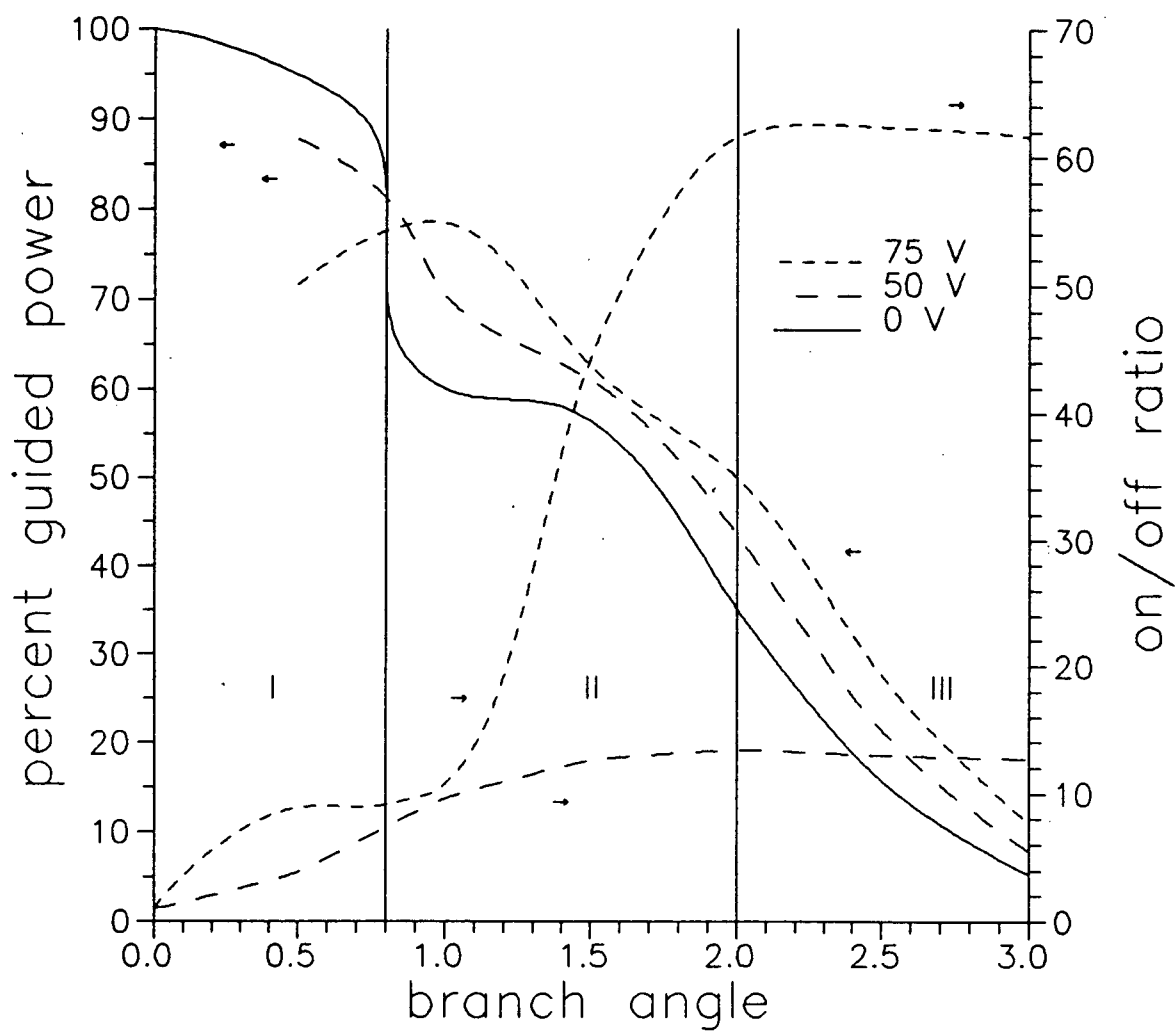
Figure 4.6 Three regions of operation as determined by branch angle

decreased in the other arm. Therefore, a net decrease in total guided power results with voltage application. The greater the voltage, the less light ends up in the weakly guiding arm, and therefore the lower the percentage guided power. Hence the power guided with no voltage applied is greater than that with 50 V applied which is greater than that with 75 V applied.

The on/off ratios in this region are low and not greatly affected by increasing the branch angle or increasing voltage. At 50 V, the on/off ratios can still be increased slightly by increasing θ because more light could still be radiated from the weakly guiding arm at this voltage. At a higher voltage, however, e.g. 75 V, the on/off ratio is saturated because more light cannot be radiated from the weakly guiding arm by merely increasing the branch angle.

As θ approaches $0.8°$, i.e., the transition between region I and region II, we see a rapid decrease in percentage guided power with no voltage applied. This sudden drop in guided power indicates that adiabatic power transfer is no longer possible. If the waveguide had been more strongly guiding, the guided power would probably drop rapidly at a larger branch angle since the optical power would be more confined, i.e., the location of this transition is dependent on fabrication parameters.

4.3.2 Region II

As we enter into region II, both the on/off ratios and the percentage guided power change their behaviours rapidly. Starting at about $1°$, the on/off ratios increase greatly and there is an increase in guided power with increasing voltage.

The performance of the modulator in this region is obviously very different from that in the previous one. Firstly, the on/off ratios are increased dramatically by applying a higher voltage and increasing the branch angle. As voltage increases, light is increasingly being channelled into the *ON* branch while being radiated from the *OFF* branch. This imbalance in power being more and more evident as θ increases because a larger percentage of the power in the *ON* branch comes from previously radiated light. (However, the total guided power still decreases with θ.) Therefore, we see a dramatic increase in the on/off ratios for 75 V applied whereas at 50 V the increase is gradual.

The amount of guided power here has a reverse trend from that in region I; the power actually increases with voltage application. Because the branch angles are fairly large in this region, a lot of light is being radiated at the junction when no voltage is applied. Upon voltage application, more light is actually steered into the *OFF* branch than is lost in the *OFF* branch. Hence, a net increase in guided power occurs. The power guided at 75 V is greater than that at 50 V, which in turn is greater than that at 0 V.

To better illustrate this increase in guided power with voltage application, Figures 4.7 and 4.8 show the optical field distributions for a 2° Y-branch modulator with a two-horn-length electrode with no voltage applied and with 50 V applied respectively. In Figure 4.7, a lot of power propagates down the centre as radiation because of the large branch angle. With voltage application in Figure 4.8, radiation is decreased and more light is guided in the signal arm.
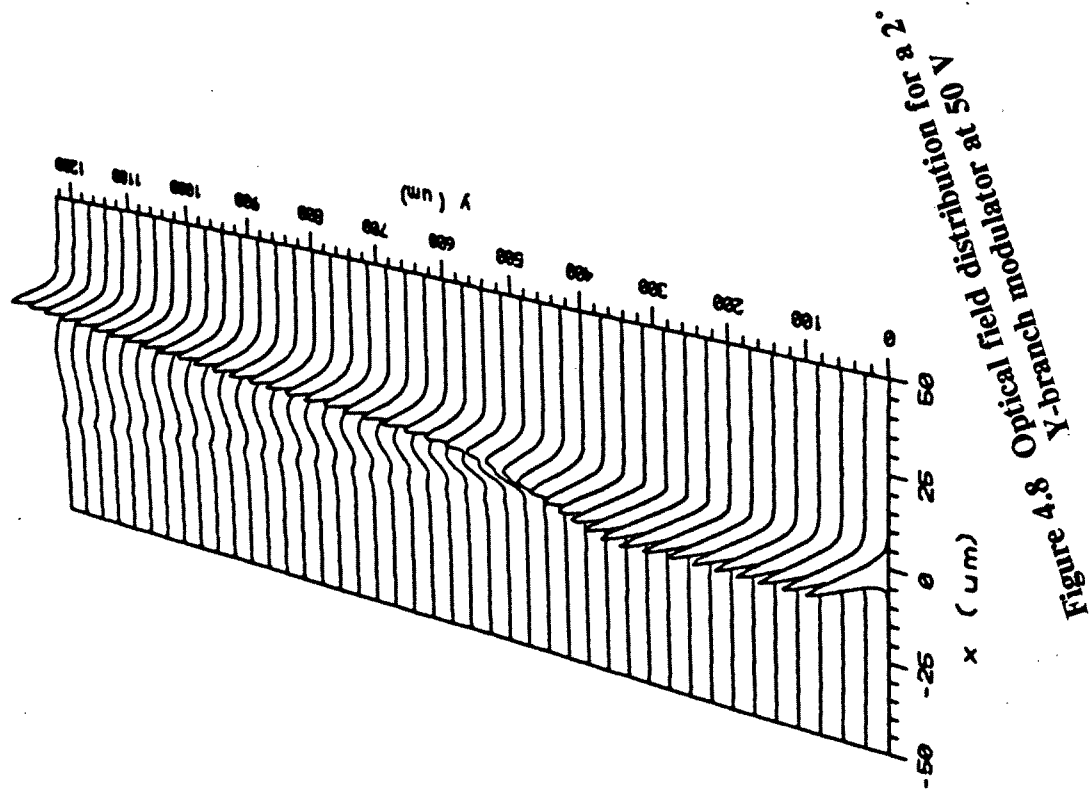
Figure 4.8 Optical field distribution for a 2°
Y-branch modulator at 50 V

Figure 4.7 Optical field distribution for a 2°
Y-branch modulator at 0 V

41
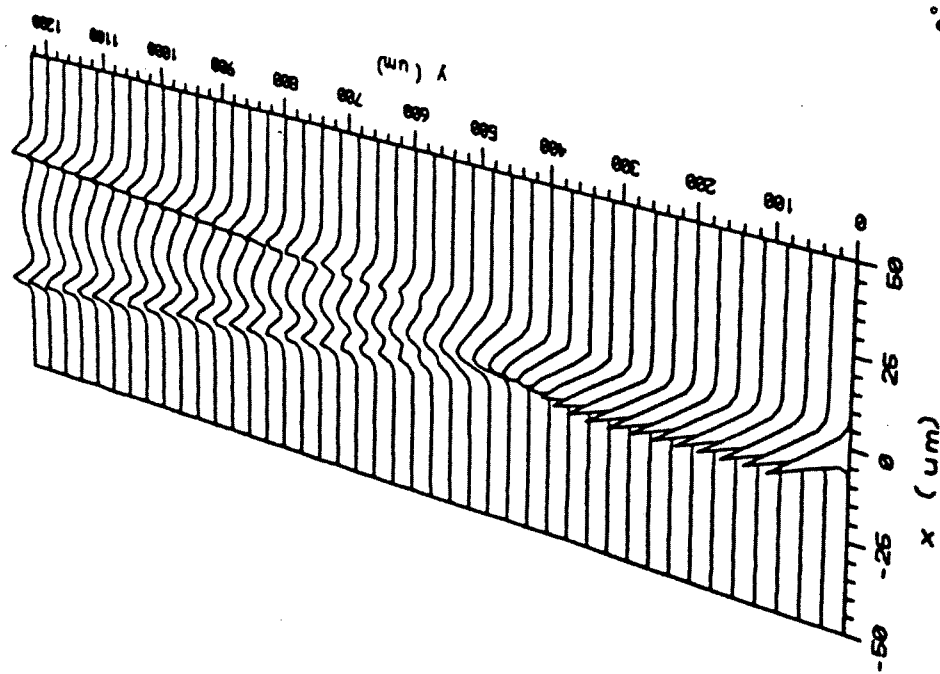
4.3.3 Region III

In this region where the branch angles are becoming increasingly large, there is a continuous decline in the amount of guided power along with a levelling off of the on/off ratios. Here, the on/off ratio actually drops slightly at 50 V, and saturates and declines slightly at 75 V as well. The saturation of the on/off ratio at 75 V is to be expected because as the branch angle continues to increase, there is so much radiation that 75 V is no longer adequate to capture the light previously lost. A higher voltage is required if the on/off ratio is to continue to increase. Basically, as the voltage increases, the saturation angle also increases. At 75 V, the saturation point occurs at $\theta = 2.0°$, whereas at 70 V, it occurs at approximately $1.5°$.

The guided power in this region is very low, e.g., as little as 12% of the power is guided for $\theta = 3.0°$ even with 75 V applied. At 0 V, the power dips down to a mere 5%. Although the guided power still increases with voltage application, the amount of power guided is too low to be useful for most applications.

4.4 Optimum Branch Angle

The optimum operating branch angle should combine a high on/off ratio and high percentage guided power. Referring to Figure 4.5, region I devices although having high percentage guided power have low on/off ratios. In region III, although the devices have high on/off ratios, the power guided is poor. Therefore, the optimum branch angle lies in region II, specifically between $\theta = 1°$ and $\theta = 1.5°$, where the on/off ratios respond

very well to increases in voltage and/or in θ. Moreover, the guided power is in the range of 80% to 60%, i.e., about -1 to -2 dB loss, which is still within the useful range. For the sake of comparison, the performance of the 1° branch modulator and the 1.5° branch modulator are examined.

With 75 V applied, the 1° branch modulator gives an on/off ratio of 11:1 and a radiation loss of 1 dB. For the 1.5° branch modulator, the on/off ratio at 75 V is 46:1, with a 2 dB radiation loss. The immediate conclusion is that by increasing the branch angle by 0.5°, we can gain 6 dB in the on/off ratio while losing 1 dB of power. Upon closer examination, however, the 1 dB loss is the total power loss, i.e., the sum of the loss from the *ON* branch plus the loss from the *OFF* branch. In fact only 0.8 dB is lost from the *ON* branch. Therefore, a 6 dB increase in on/off ratio is gained for a loss of 0.8 dB from the *ON* branch.

Depending on the application, the optimum angle lies somewhere between 1° and 1.5°. For applications where the amount of guided power is more crucial than a high on/off ratio, a 1° branch modulator may suffice. For applications which require a higher on/off ratio, the 1.5° branch modulator would be more suitable.

To summarize the layout and fabrication parameters of a Y-branch modulator based on the simulation results (using a 1.5° branch angle as the optimum), Figure 4.9 shows the plan view and cross-sections of the modulator. Table III shows the corresponding fabrication parameters for this modulator.
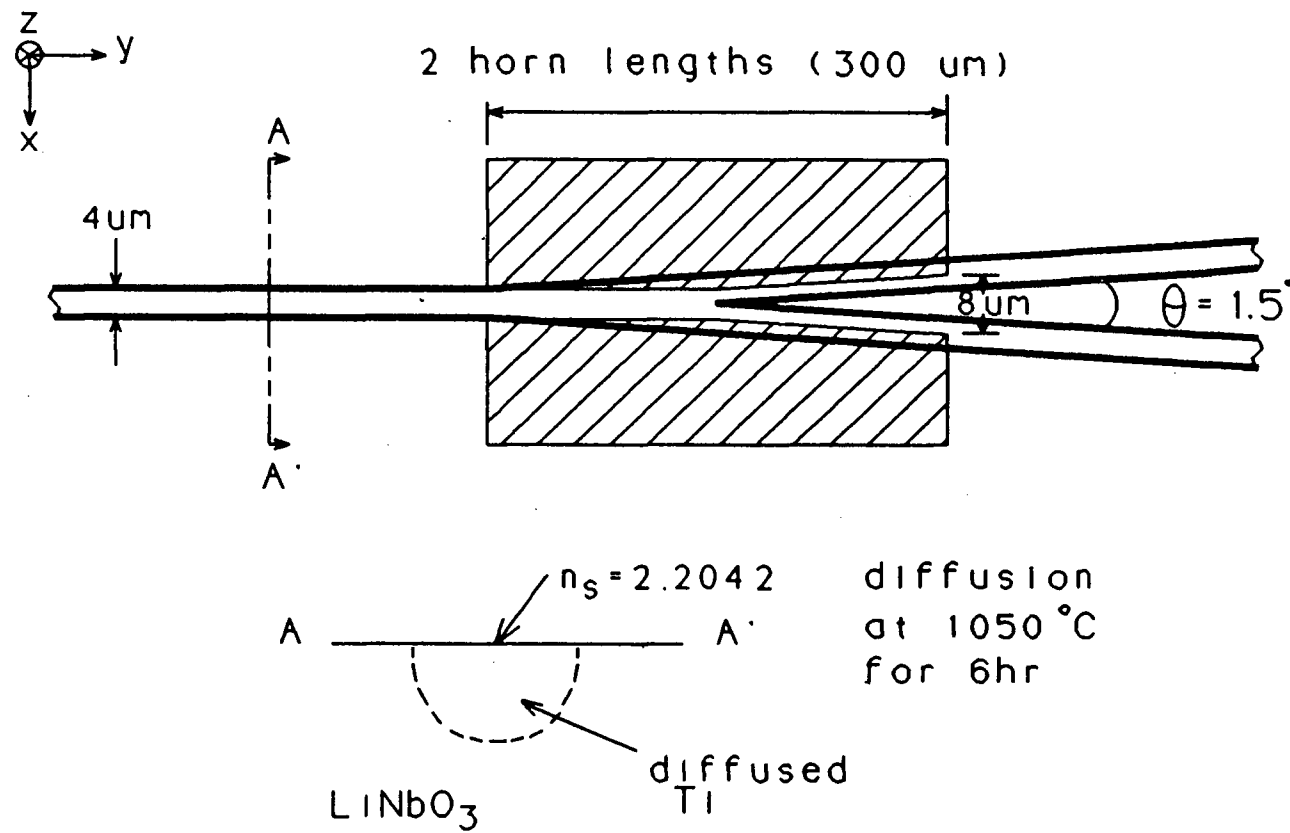
Figure 4.9 Device layout of a 1.5° Y-branch modulator

Table IV Fabrication parameters of a 1.5° Y-branch modulator

Titanium thickness	480Å
bulk refractive index n_b	2.2
maximum refractive index n_s	2.2042
diffusion depth D	3 μm
diffusion temperature	1050°C
diffusion time	6 hrs
SiO$_2$ buffer layer thickness	2000Å
Aluminum thickness for electrodes	4000Å
waveguide pattern width W	4 μm
branch angle θ	1.5°
electrode gap at input	4 μm
electrode gap at output	8 μm
electrode length	300 μm

With an electrode length of 300 μm, the calculated capacitance [10] is approximately 0.117 pF (appendix A), assuming the width of the electrode is five times that of the width. Such low capacitance promises switching speeds in excess of 50 GHz, which would make it one of the fastest electro-optic modulators reported to date.

Chapter V Device Fabrication

To verify the simulation results Y-branch electro-optic modulators are fabricated on z-cut LiNbO$_3$. Masks for the Y-branch waveguides and electrodes, respectively, are designed. Attempts are made to circumvent fabrication problems previously encountered.

5.1 Mask Design

For the mask design, the Y-branches step out at 0.2 μm steps rather than 0.1 μm as specified in the simulations. This is done in order to keep down the cost of the masks, moreover, the performance of the Y-branches are not supposed to be adversely affected by using 0.2 μm steps [29]. Due to the tight tolerances and small dimensions required for the masks, an electron-beam mask is chosen over one which is optically pattern generated.

The Y-branch and electrodes were designed using the CAD package ICED by IC Editors, Inc. For the waveguide mask, straight waveguides are placed between the Y-branches so that measurements of the percentage guided power can be made by comparing the power guided in the adjacent straight guides with that in the Y-branch. The output branches are placed 50 μm apart from each other and the total length of the waveguides is 13 mm. The branch angles used in the mask are 0.5˚, 1.0˚, 1.5˚, 2.0˚, 2.5˚, and 3.0˚. Markers are placed both on this mask and the electrode mask for alignment purposes. The electrodes are placed in an interdigitated fashion for ease of voltage application through probes. The interconnecting lines are 50 μm wide so that

they are less prone to damage. The pads have a minimum size of 0.5 mm x 0.5 mm. Two sets of electrodes are designed for the Y-branch waveguides: two-horn-length electrodes, and three-horn-length electrodes.

The two electron-beam masks are fabricated by Tektronix, Oregon, USA, on anti-reflection sodalime glass 3/16" thick. A 0.2 μm spot size is used for writing the pattern.

5.2 Fabrication Problems

A previous group at UBC had tried to fabricate waveguides on z-cut LiNbO$_3$ [30], and encountered two main problems: dust accumulation on the crystal due to electrostatic attraction, and out-diffusion of LiO$_2$ causing unwanted surface guiding. Therefore, before fabricating the devices using the waveguide and electrode masks, a trial run fabrication is performed using an existing lower quality Y-branch mask to investigate these two fabrication difficulties, with the goal of eliminating them [31].

The dust accumulation, due to electrostatic attraction, is a result of LiNbO$_3$'s pyroelectric effect. As the crystal experiences temperature changes, an internal electric field builds up which attracts dusts and air-borne particles, which are almost impossible to remove. This pyroelectric effect is especially strong for z-cut crystals. Utmost care must therefore be taken to assure that dust does not accumulate on the surface of the crystal where the waveguides reside prior to diffusion. By minimizing open-air exposure of the crystal, by using either Dust-Off or nitrogen to blow off dust during each fabrication step, and by limiting the time required to do an entire fabrication, we manage to reduce dust particles on the waveguides and produce a higher yield during fabrication.

5.2.1 LiO$_2$ Out-diffusion

Compared to dust accumulation, the formation of surface waveguides due to LiO$_2$ out-diffusion is a more serious problem because it causes radiation loss and crosstalk between devices. Although it is a common problem encountered when forming channel waveguides through diffusion of Ti into LiNbO$_3$ under high temperature, the methods reported for combating it are numerous and at times contradictory [32,33]. Diffusion of Ti in a dry sealed atmosphere for 8 hours at 1050°C has worked for Neyer *el al.* [34], and a similar dry diffusion performed at 980°C for 10 hours using LiNbO$_3$ powder has worked for Esdaile [35]. However, past experience at our laboratory indicates that dry diffusion always results in surface waveguides.

Diffusion in the presence of water vapour has suppressed LiO$_2$ for some [36,37] but not for others claiming to have performed the diffusion under identical conditions [38]. Diffusion temperature and humidity seem to be the crucial factors in this method. Because the wet diffusion method has been reported to be consistently successful [32] and has been able to suppress LiO$_2$ out-diffusion once in our laboratory, we decided to pursue this method of diffusion in the presence of water vapour with flowing oxygen. Although Canali *et al.* [39] have found that water vapour may damage the surface of the crystal, we have not yet noticed any adverse effect on our experimental results from wet diffusion, possibly because our measurements are relative.

We performed our diffusion in the presence of wet O$_2$ flowing at a rate of 1.5 L/min. The O$_2$ is saturated with water vapour by bubbling it through a column of water 7.5" high heated to 80°C. The water temperature is monitored and maintained so that

the humidity of the O_2 is constant. The gas is bubbled through the water by using a 500 mL gas bottle equipped with a fritted cylinder. The water level is kept constant by adding heated water at approximately 45 min intervals. In any case, the water level never dips below 7". The furnace is heated at a rate of about 13°C/min and the diffusion takes 6 hours at 1050°C, following which the furnace cools off at about 9°C/min to its initial room temperature.

The experimental setup is shown in Figure 5.1. Using the above method, we have been able to consistently produce waveguides with very little surface guiding.
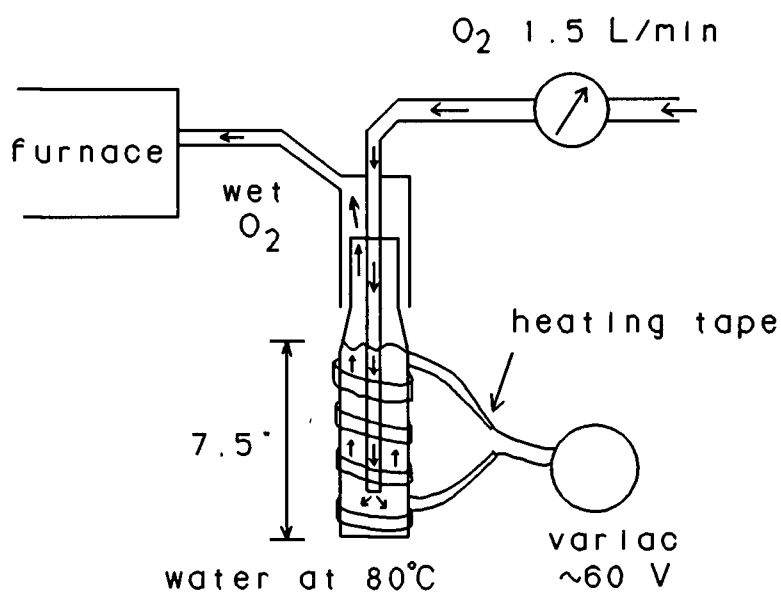
Figure 5.1 Setup for diffusion under wet oxygen flow

5.3 Fabrication Procedures

Using optically polished z-cut $LiNbO_3$ wafers from Crystal Technology, we begin by evaporating a layer of aluminum (Al) about 0.5 μm thick onto the wafer for protection. Then we cut the wafer into quadrants using an abrasive slurry wire saw (South Bay Technology model 850). The wafer is mounted onto a graphite block using wax for the cutting procedure. A steel wire 0.015" thick along with an abrasive consisting of de-ionized (DI) water, glycerine, and 600 grit silicon carbide are used. After cutting, the working quadrants are cleaned in a solution of warm trichloroethylene to remove the wax, followed by a warm solution of Alconox cleansing agent to remove any dirt accumulated during the cut. Then the protective Al layer is removed by using an Al etch solution consisting of 57 mL DI water, 21 mL nitric acid (HNO_3), and 222 mL phosphoric acid (H_3PO_4), following which the wafers are given a DI water bath. Before loading the wafers into the Carl Herman & Associates (CHA) vacuum thermal evaporation system for Ti evaporation, they are immersed in methanol for transportation to the CHA. This is done to minimize exposure of the bare wafers to air prior to Ti deposition since the wafers should ideally be dust-free before the deposition. As the wafers are taken out of methanol they are air blown dry to remove any particles.

Using only one Ti coil for the evaporation, a layer of Ti about 500Å thick is deposited on the wafers. The wafers are subsequently removed from the CHA and immediately transferred, in a covered beaker, to the yellow room for patterning.

After air-blowing the wafers, Shipley positive photoresist PR 1400-27 is spun onto them at 4000 rpm for 40 sec giving a layer of photoresist approximately 1.5 μm thick. The samples are then pre-baked at 70°C for 30 min. After cooling the samples the waveguide mask is used to pattern the Y-branch pattern onto the samples using a Karl-Süss MJB3 contact mask aligner. The pattern is aligned on the samples such that the waveguides are parallel to a straight edge so that all the guides would be either x- or y-propagating. The photoresist is exposed for 23 sec under intense light of 25 mW/cm^2 from a mercury lamp. Then they are developed in cold Microposit developer MR-312 (50% concentration) for 1 min, and rinsed in a DI water cascade bath. If the Y-branch waveguide patterns look good upon examination under the microscope the next step is to remove the excess Ti so that only a waveguide pattern of Ti is left behind.

Using a plasma deposition/etching system (AMNS-500E by Plasma-Therm Systems), the exposed Ti is etched in a freon 14 plasma at 60°C for 20 min at a power density of 0.20 W/cm^2. A loading factor of 90 and a tuning factor of 83 are used to minimize reflected power. The photoresist, having been exposed to freon 14 in the plasmatherm, now has hardened and requires a solution of Microstrip 2001 solvent to remove it. By submersing the samples in Microstrip 2001 and heating the solution to its boiling temperature of 85°C, then rinsing the samples in two warm baths of DI water, the photoresist is stripped and only a Y-branch waveguide pattern of Ti is left behind on the crystal surface. A profilometer (Tencor alpha-step 200) is used to measure the Ti thickness before diffusion and shows a Ti thickness of about 500Å. The waveguide widths are measured under the microscope and the 4 μm guides are found to be slightly

wider than 4 μm but no wider than 4.5 μm. The increase is expected and unavoidable due to the use of positive photoresist. Figure 5.2 shows the Ti patterns for all the 4 μm branches prior to diffusion, Figure 5.3 shows the Ti patterns for the previous sample with the 1.5° and 2° branches. The patterns are almost dust-free and they are ready to be placed in the furnace for Ti diffusion.

The diffusion process is as explained in section 5.2.1 with the high humidity O_2 flowing through the oven at 1.5 L/min. After heating at 1050°C for 6 hours, all the Ti has been diffused into the wafers to form waveguides. After cooling, the samples are taken directly from the diffusion oven to the sputterer for deposition of an optical buffer layer of SiO_2. The sputterer is a Perkin Elmer Sputtering System model 3140.

After loading the samples the sputter target is first sputtered for 1 hour for pre-cleaning, then the SiO_2 target is sputtered using 18 mtorr of argon and 5 mtorr of oxygen at 0.55 W/cm^2 until the desired SiO_2 thickness is deposited.

Before loading the samples into the CHA for Al evaporation to form the electrodes, the samples are immersed in a solution of isopropanol to discharge any built-up charges and dislodge any foreign particles. As before, the samples are taken directly out of the isopropanol, blown dry, and placed into the CHA. Approximately 4000Å of Al is deposited on the samples. Two Al coils are used during the process.

To pattern on the electrodes, Shipley PR 1400-27 photoresist is spun on the samples at 4000 rpm for 40 sec, followed by a pre-bake at 70°C for 30 min. The electrode mask is subsequently aligned on the samples such that the markers on the mask are matched with those on the samples, and they are exposed and developed. The
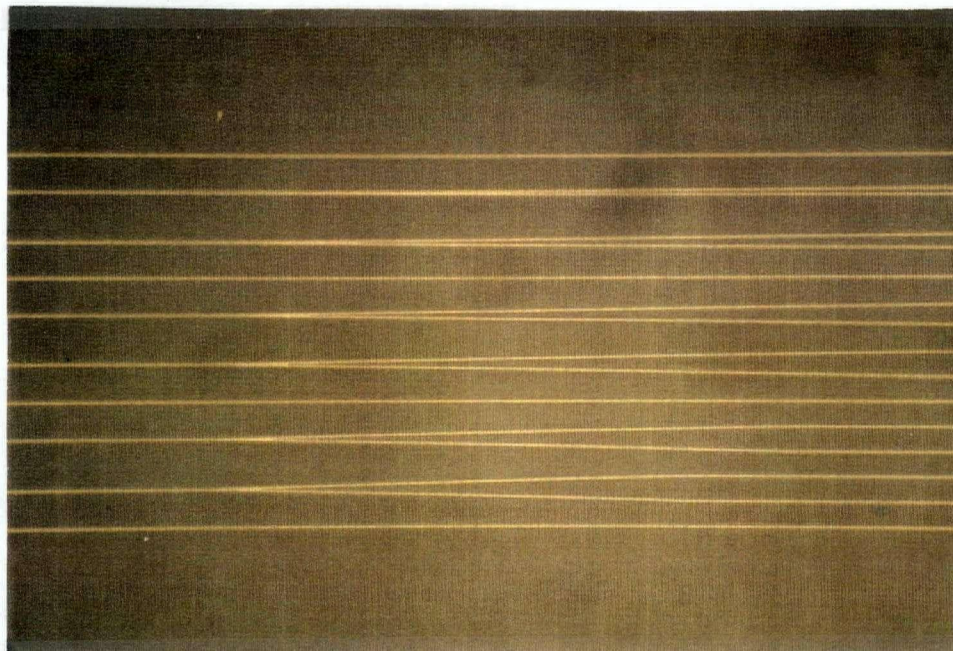
Figure 5.2 Ti Y-branch patterns prior to diffusion
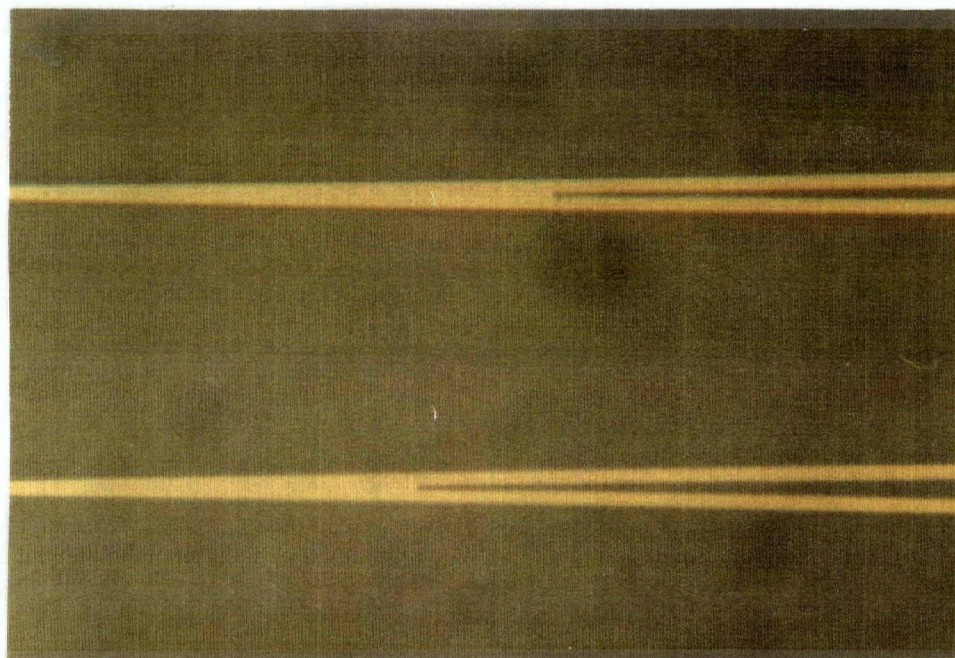
Figure 5.3 Ti Y-branch pattern for 1.5° and 2.0° branches prior to diffusion

samples are then put through a DI water cascade bath, followed by post-baking at 110°C for 20 min to harden the photoresist pattern.

Excess Al which is not covered by the photoresist is removed by using the Al etch solution mentioned earlier, followed by a DI water bath. Now that the Al electrode pattern is formed on the samples, the residual photoresist is removed with boiling Microstrip 2001 (at 85°C), followed by a water bath at almost the same temperature to rinse off the solvent. Care should be taken when transferring the samples from the Microstrip 2001 to the warm water bath, because past experience has shown that an Al etching solution forms when 5 mL (or more) of Microstrip 2001 is mixed with 1 L of water. Therefore single sample holders should be used rather than basket holders since single holders retain less liquid. Also only one sample should be rinsed per beaker so that the concentration of Microstrip 2001 is kept as low as possible in the rinsing water.

The final patterns on the samples are shown in Figures 5.4 and 5.5 which show all the 4 μm Y-branch modulators and the 2° Y-branch modulator respectively. Due to the use of a chemical wet etch in removing excess Al to form the electrode patterns, the electrode gap widths are slightly wider than the 4 μm gap specified on the electrode mask.

In order to test the samples, they need to be cut to size and optically polished. The cutting procedure with a wire saw is as documented earlier in this section, and each sample is cut into halves. For polishing, a Buehler polisher is used. The sample is mounted onto another piece of $LiNbO_3$ using wax, with the waveguide side against the other piece of $LiNbO_3$. They are then clamped down onto the polishing jig, exposing

only about 1 mm of the end for polishing. Standard polishing procedures are used to optically polish the input and output ends of the samples so that no scratch is within 20 μm of the surface where the waveguides reside. When the samples are polished, they are soaked in a solution of warm trichloroethylene to remove the wax, and then in methanol to remove any other particles. Care must be taken not to scratch and damage the electrodes when handling the samples.
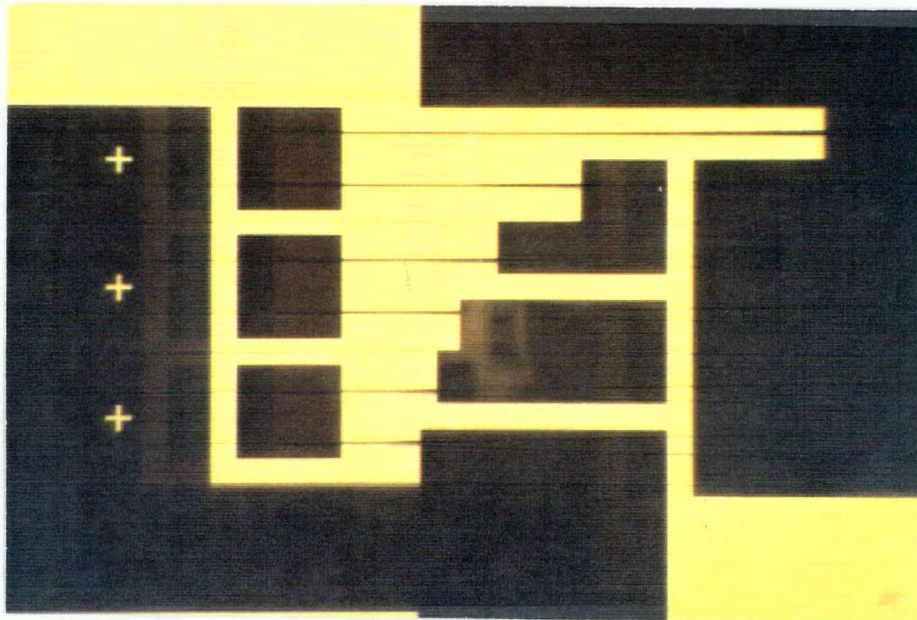
Figure 5.4 Completed modulators with two-horn-length electrodes
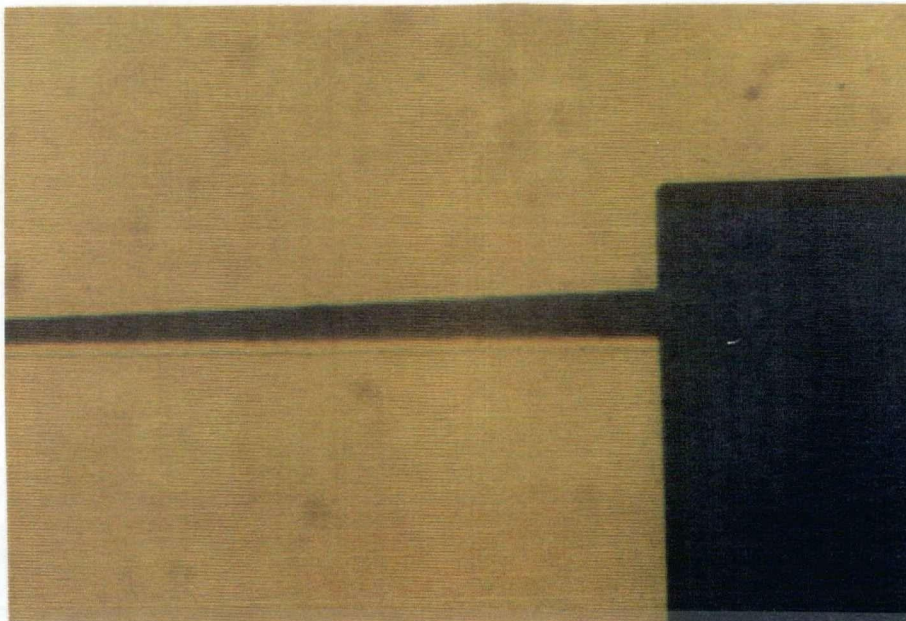
Figure 5.5 Completed 2° Y-modulator with two-horn-length electrode

Chapter VI Device Testing and Measured Results

6.1 Experimental Setup

In order to compare the experimental results with the simulated results, the fabricated samples are tested for their on/off ratios and percentage guided power. The entire experiment is performed and setup on an optics bench to dampen external vibrations which could adversely affect the measurement. Figure 6.1 shows the experimental setup used.

Polarized light from a Helium-Neon (HeNe) laser at 632.8 nm is focused through a 20X objective into single mode polarization-maintaining optical fibre (Newport F-SPV 630 nm). At both ends of the fibre, the cladding is first softened via dipping into a solution of trichloroethylene then removed with a clean tissue. The bare fibre is then cleaved to provide a smooth facet for efficient coupling of light. The output end of the fibre is placed on a fibre alignment micropositioner which allows for six degrees of freedom for manipulation. The fibre is aligned with the laser and the test sample such that polarized light is emitted from the fibre and launched into the TM mode of the waveguides. The extinction ratio for this polarized light is measured to be 100:1.

The sample is placed on an aluminum platform and the fibre is brought to close proximity to but not in contact with, the input edge of the sample. The output light from the waveguide is focused through a long focal length 25X objective onto the detector. The objective is supported by a three-way translational stage to provide adequate manipulation of movement. A polarizer is placed at the output of the objective to remove

the small signal that may result from the light coupled into the TE mode. A pinhole is placed in front of the detector serving as an aperture. Two pinhole sizes are used: one for measurement without voltage, which is 1.0 mm in diameter, the other is for measurement with voltage application, which is 0.4 mm in diameter (see section 6.2.1). The detector consists of a silicon photodetector (Newport 818-SL) and a laser pico-watt digital power meter (Newport 835). The data from the power meter is sent to a HP 54600A digital oscilloscope, where it can be stored and loaded into an ASCII file on a PC.

The modulating voltage is a slowly-varying triangle wave, applied to the waveguide electrodes via a pair of probes. The power launched into the waveguides is on the order of μW, reducing the photorefractive effect. The response of the detector is slow at these power levels, e.g., 3 msec for the 20 μW range, therefore the modulating voltage should be low frequency. We used a 1 Hz signal.
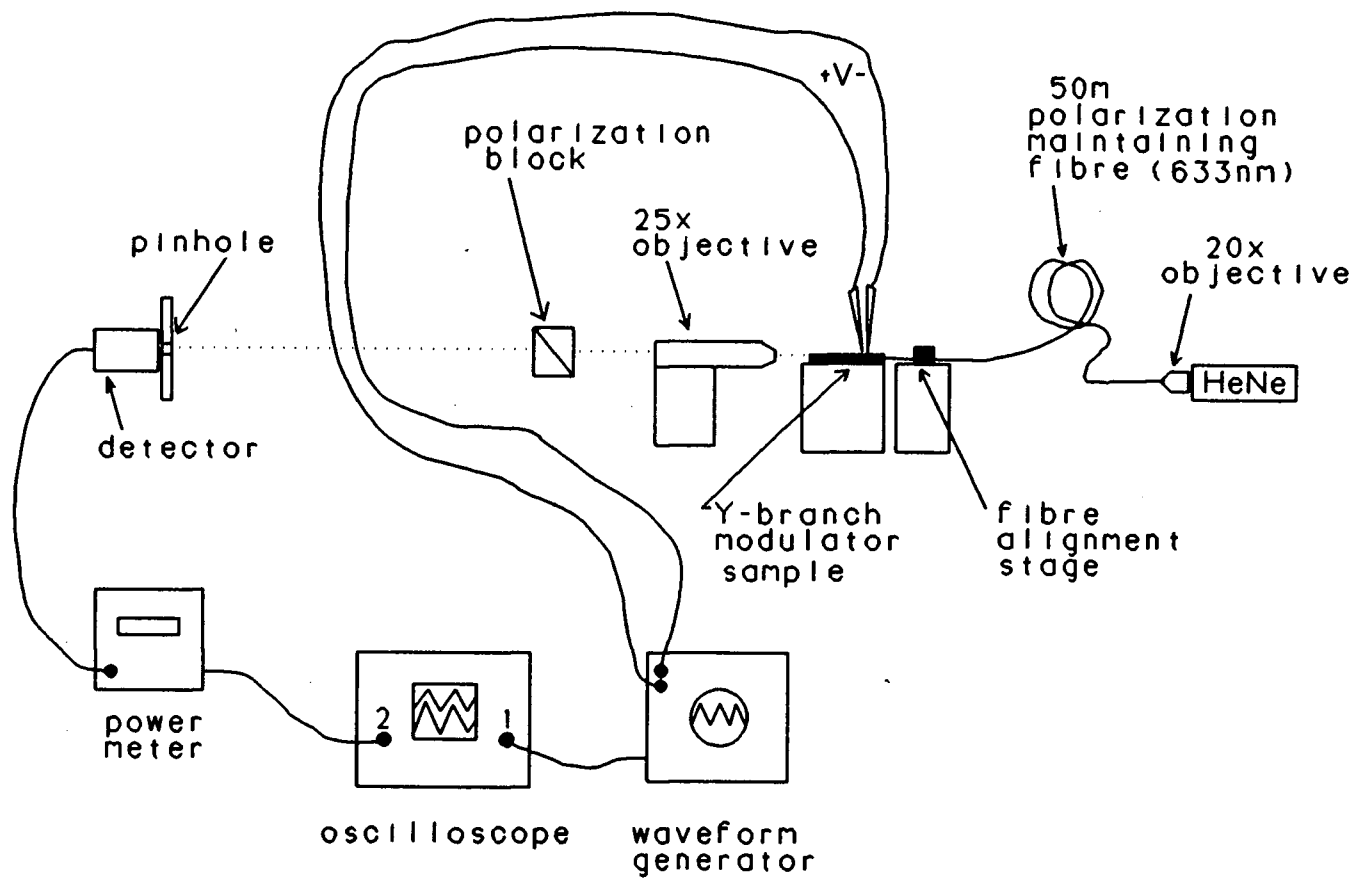
Figure 6.1 Optical bench test setup

pinhole

detector

polarization
block

25x
objective

50m
polarization
maintaining
fibre (633nm)

+V-

20x
objective

HeNe

Y-branch
modulator
sample

fibre
alignment
stage

power
meter

oscilloscope

waveform
generator

6.2 Measurement Techniques

We tested the devices sequentially; the order of testing is straight waveguide, $0.5°$ device, $1.0°$ device, straight waveguide, $1.5°$ device, $2.0°$ device, straight waveguide, $2.5°$ device, $3.0°$ device, straight waveguide. For the straight waveguides, the fibre is first aligned such that there is maximum light output. Using the 1.0 mm pinhole, the power is measured and recorded directly from the power meter. For each Y-branch modulator, however, the fibre has to be aligned such that an equal and maximum amount of light is guided by each branch arm. The power is then measured and recorded; this measurement is also performed with the 1.0 mm pinhole. Then the modulating voltage is applied and the output from the branch arms is recorded one at a time on the oscilloscope; the 0.4 mm pinhole is used for measurement in this case (see section 6.2.1 below). Figures 6.2 (a) and (b) show the light spots projected from the output of the $1.5°$ modulator as seen on a screen placed at the detector. (Here, the spots were not balanced using the detector but by eye). Figure 6.2 (a) is for the case with no voltage application, and hence nearly equal intensity. Figure 6.2 (b) is for the case with 75 V applied; one arm is turned off while the other is increased in intensity.

Figure 6.3 shows a typical output response of a Y-branch modulator as a modulating voltage is applied. In this case, it is a $1.5°$ Y-branch with a 75 V triangle wave applied. The top trace is the applied voltage, and the bottom trace is the output light intensity of one of the branch arms. If the other branch arm is recorded instead of this one, then the response would have been phase shifted by $180°$. The on/off ratio is the ratio of the maximum power to the minimum power.

60
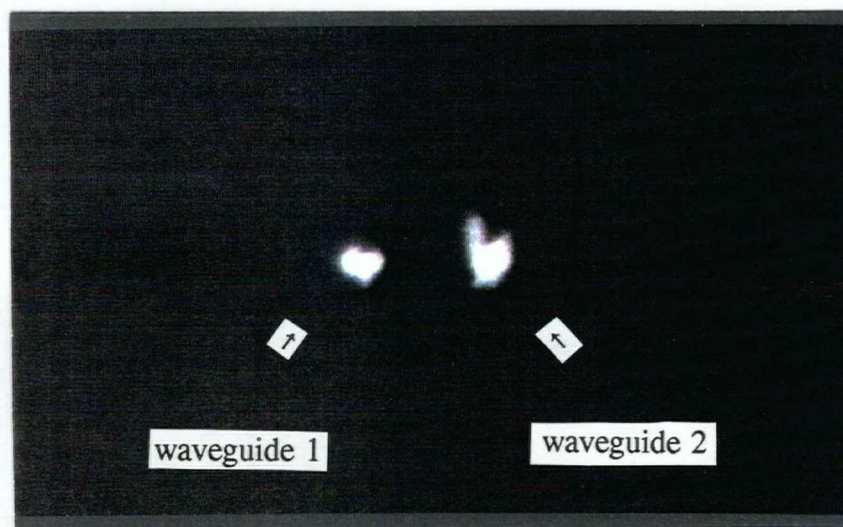
Figure 6.2 (a) Light output from the 1.5° Y-branch
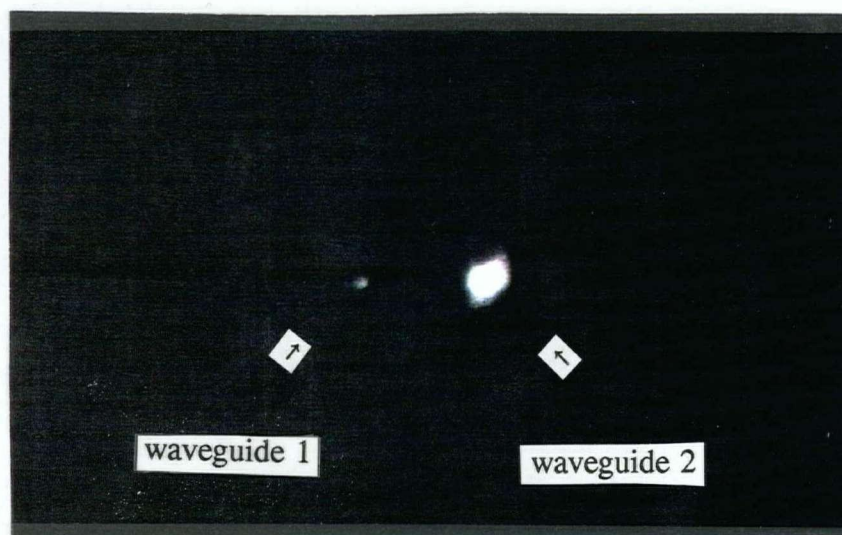
Figure 6.2 (b) Light output from the 1.5° Y-branch modulator with 75 V applied

We measured the percentage guided power by comparing the sum total power at the two outputs of the modulator to the power out of the adjacent straight waveguide. Since the straight waveguide is adjacent to the modulator, both waveguides are assumed to have nearly identical guiding characteristics. First, the output powers from the Y-branch and the straight waveguide are maximized at 0 V by properly aligning the fibre. The two respective power levels can be read directly from the power meter and the percentage guided power for cases with no voltage application can be calculated. Then voltage is applied and the data is read off the oscilloscope. The power meter is calibrated and corresponds to 27 μW/V in the 20 μW range, and 2.7 μW/V in the 2 μW range. Based on these calibrations, the data recorded on the oscilloscope can be converted back to power levels.
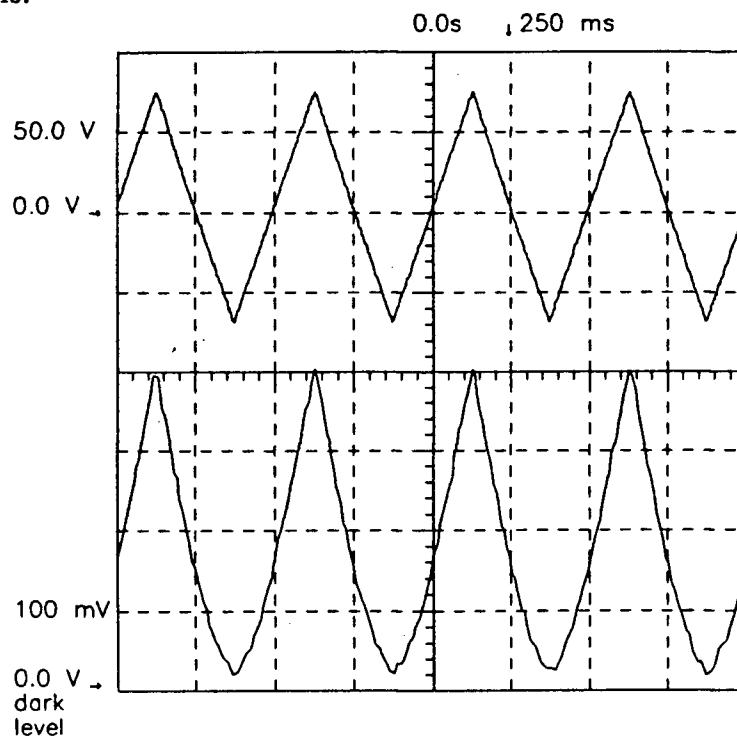
Figure 6.3 Output response of the 1.5° Y-branch modulator with a modulating voltage of 75 V

6.2.1 Compensating for Radiation Modes

The pinholes are used so that only power in the guided modes is picked up by the detector. For measuring the percentage guided power, especially with no voltage applied, the 1.0 mm pinhole is adequate since the power in the radiation modes is small compared to the guided power. The image projected onto the pinhole is 40X the actual size, therefore the 1.0 mm pinhole corresponds to an aperture size of 25 μm which allows interrogation of the entire output spot. However, for measurement of the on/off ratio, any radiation mode power can distort the results. A smaller pinhole, 0.4 mm, which corresponds to an aperture of 10 μm, is used in this case to filter out much of the radiation modes. Figure 6.4 shows the electric field component of the optical distribution at the output of a 1.5° branch modulator with 75 V applied. Evidently, the aperture size will affect the on/off ratio measured.

Here, we define a "bulk" on/off ratio as the measured on/off ratio, which is the ratio of the total powers, containing both the guided mode and the radiation modes, in the *ON* branch and the *OFF* branch respectively. The "true" on/off ratio is defined as the ratio of the powers only in the fundamental TM-like mode of the *ON* and *OFF* branches; this is the ratio predicted by the numerical simulations. If we examine the simulation results, and take into account the straight sections of the branch arms (which the initial simulations did not do due to increased computational time), the bulk on/off ratio can be found by first calculating the powers in a 10 μm window centred about the outputs of the *ON* branch and the *OFF* branch respectively. Since both of these powers contain the guided mode and the radiation modes, these power levels are what would be

measured by the detector. Because the power from radiation modes constitutes a greater portion of the total branch power in the *OFF* branch than the *ON* branch, the on/off ratio evaluated by taking a ratio of these two powers, i.e., the bulk on/off ratio, is obviously less than the true on/off ratio. Figure 6.5 shows the bulk on/off ratio as a percentage of the true on/off ratio for a 10 μm aperture as a function of branch angle for 75 V applied. Evidently the bulk on/off ratio decreases as θ increases because of increased radiation.

Compensation for the inclusion of radiation modes in the measurements is also required for the percentage guided power. The bulk percentage guided power, which includes both guided and radiated modes, does not differ very much from the true percentage guided power for branch angles less than or equal to 2.0°. For larger branch angles, the bulk value is significantly greater due to increased radiation, e.g., over three times greater for $\theta = 3.0°$ with no voltage applied.
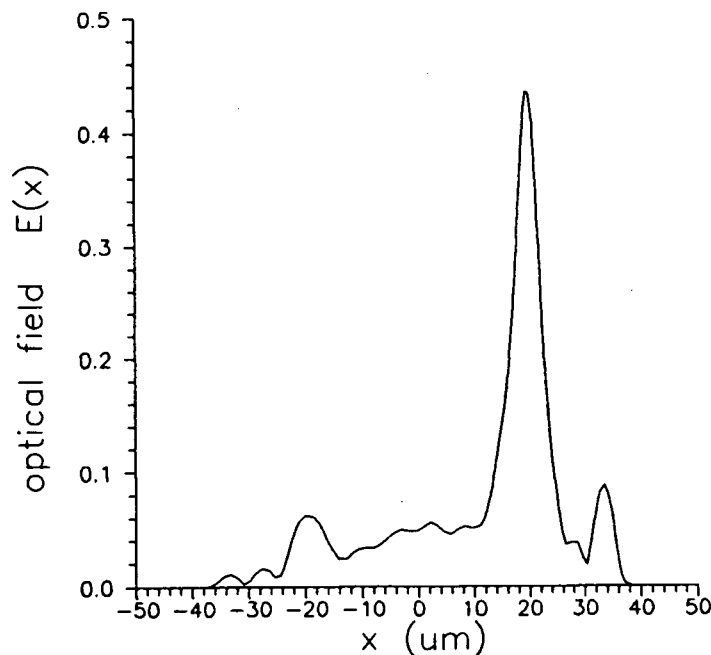
Figure 6.4 Optical field of the 1.5° Y-branch modulator with 75 V applied
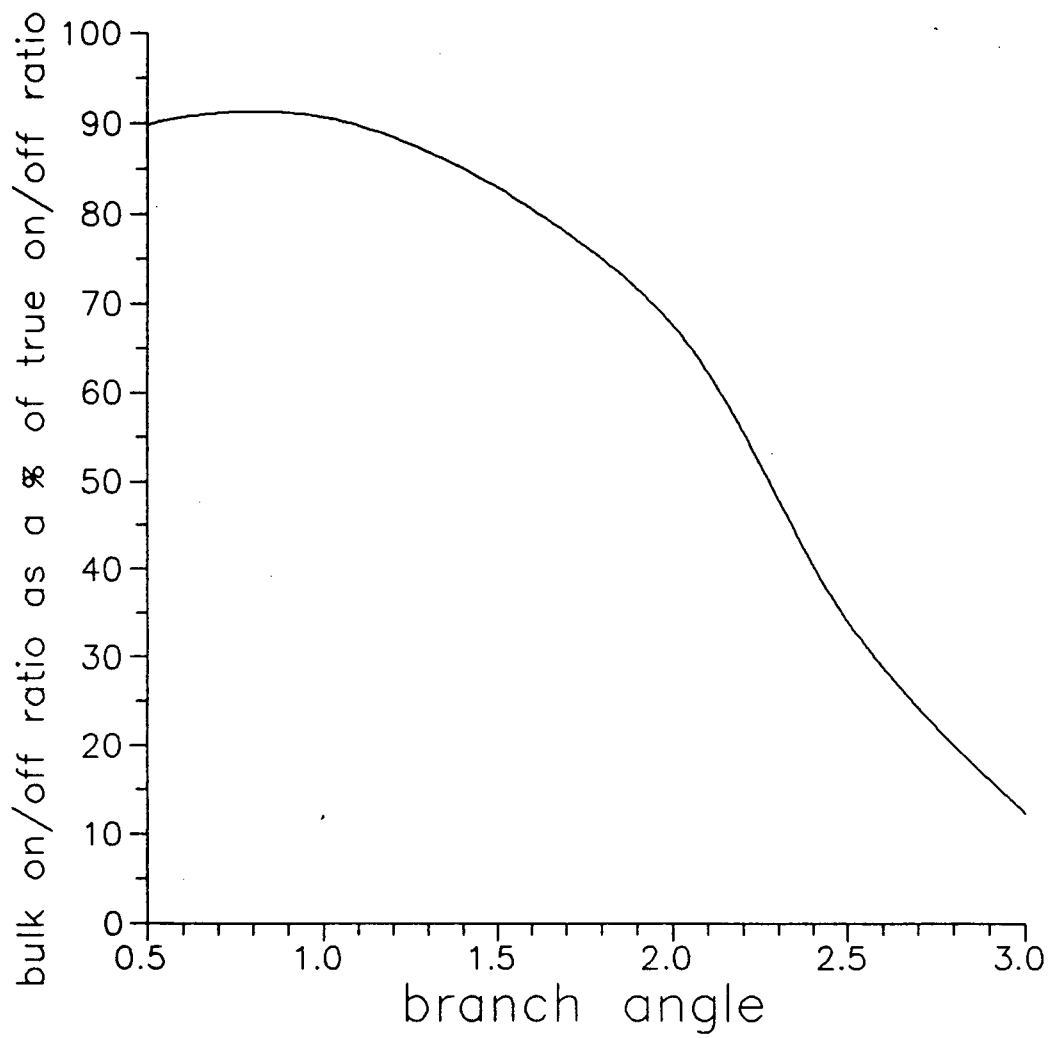
Figure 6.5 Bulk on/off ratio vs. branch angle θ with 75 V applied

6.3 Measured Results

The measured results, when compensated for the effects of the radiation modes, are tabulated in Tables V-VIII with the theoretical results shown for comparison. Tables V and VI show the on/off ratios and percentage guided power for the two-horn-length electrode respectively, while Tables VII and VIII show the three-horn-length electrode results. The transfer characteristics for the 1.5° branch is illustrated in Figures 6.6.
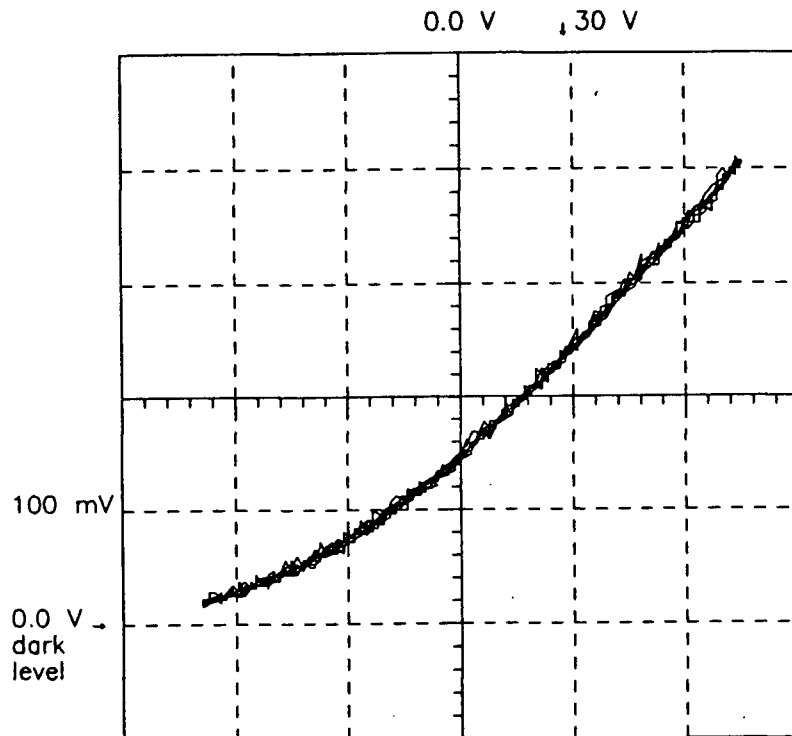
Figure 6.6 Transfer characteristics of the 1.5° Y-branch modulator with a two-horn-length electrode

Table V On/off ratios with two-horn-length electrode

Θ	50 V		75 V	
	theoret-ical	experi-mental	theoret-ical	experi-mental
0.5[*]	3.9	3.8	8.9	8.1
1.0[**]	9.6	10.0	11	16
1.5	12.6	10.2	44	40
2.0[**1]	13.4	12.5	62	59
2.5	12.4	12.2	62	49

Table VI Percentage guided power with two-horn-length electrode

Θ	0 V		50 V		75 V	
	theoret-ical	experi-mental	theoret-ical	experi-mental	theoret-ical	experi-mental
0.5	95%	93%	87%	---	72%	---
1.0[**]	60%	63%	70%	69%	79%	80%
1.5	56%	57%	61%	64%	62%	66%
2.0[**1]	35%	36%	44%	39%	50%	47%
2.5	16%	14%	21%	19%	28%	24%
3.0	5%	5%	---	---	---	---

1. Reference [40].

[*] Set C, 3.2 μm waveguide.

[**] Set A, with 670Å thick of SiO_2.

Table VII On/off ratios with three-horn-lengths electrode

Θ	50 V		75 V	
	theoret- ical	experi- mental	theoret- ical	experi- mental
1.0	9.6	4.3	15	8
1.5	10.8	5.1	23	19
2.0**	12.1	13.1	49	52
2.5**	12.0	12.5	50	53

Table VIII Percentage guided power with three-horn-length electrode

Θ	0 V		50 V		75 V	
	theoret- ical	experi- mental	theoret- ical	experi- mental	theoret- ical	experi- mental
1.0	60%	82%	70%	65%	78%	76%
1.5	56%	55%	56%	58%	53%	57%
2.0**	35%	35%	43%	41%	49%	46%
2.5**	16%	13%	---	---	---	---
3.0	5%	5%	---	---	---	---

6.4 Discussion of Results

Comparing the theoretical values to the experimental values in Tables V-VIII, they agree reasonably well in general. Some factors which contribute to the discrepancies between the two include imperfect fabrication, and the 0.2 μm rather than 0.1 μm step size at which the Y-branches spread out. The HeNe laser has a $\pm 3\%$ dc drift over a period of several minutes, and the photodetector response can also vary by $\pm 3\%$, which can easily account for the differences in the percentage guided power. One problem that may be encountered during fabrication is the misalignment of electrodes to the waveguides. Yet as we postulated, the device performances are not very sensitive to these fabrication variations, as our experimental results clearly demonstrate.

There are three sets of samples measured, which differ in the thickness of the SiO_2 optical buffer layer and waveguide width. The ones with an "**", called set A, have a SiO_2 thickness of about 670Å; the others, called set B, have about 2700Å. Set C, the only one with an "*", is a 3.2 μm waveguide with 2700Å thick of SiO_2; all other waveguides are 4 μm. Otherwise, the fabrication parameters are identical. Since the simulations were computed at 2000Å thick of SiO_2, the measured on/off ratios for set B should be slightly lower because the thicker the oxide layer results in a weaker modulating field and hence a slightly smaller change in the refractive index. Set A, however, due to the thinner oxide layer, should have higher on/off ratios than predicted. They also should have lower percentage guided power due to more loss in the TM-like mode as a result of the thin oxide layer. These trends are reflected in Tables V-VIII,

with set A modulators mostly having slightly lower on/off ratios than predicted, and set B modulators mostly having higher on/off ratios but less guided power than predicted.

6.4.1 Percentage Guided Power

The percentage guided power for both of the electrode lengths are generally in very good agreement with the theoretical values from the simulations. The major discrepancy occurs at 1.0°, where the 0 V guided power is exceedingly high for one set of data. Recalling Figure 4.4 which shows the percentage guided power as a function of angle θ, a rapid transition occurs at about 0.8° for a $\Delta n_s = 0.0042$. The location of this transition presumably will be most sensitive to the fabrication parameters, since the grazing incidence for total internal reflection of a guided wave is highly dependent on Δn_s [18]. If this assumption is true, then the value of 81.5% guided power is reasonable for the 1.0° Y-branch device.

The guided powers for the 0.5° modulator at 50 V and 75 V are not available because all the 0.5° Y-branch modulators fabricated turned out to be multi-mode rather than single-mode. Using 4 μm strips of 500Å thick Ti for diffusion might have produced waveguides which support a second mode, here the strips usually turn out to be slightly greater than 4 μm (see Fabrication Procedures in section 5.3). The second mode is not detected at other branch angles, possibly because the larger branch angle devices filtered out the power coupled into higher order modes. Using 3.2 μm wide Ti strips for the indiffusion, however, gave single-mode operation at 0.5° branch angle.

The guided power for the 3.0° Y-branch modulator is also not available for cases with modulation because of excessive radiation, resulting in too little guided power at the output. The readings from the oscilloscope are very distorted. Also it is very difficult to compensate for the radiation modes when they comprise such a large portion of the output power.

6.4.2 On/off Ratio

The on/off ratios shown in Tables V and VII give very encouraging results. The theoretical and experimental values generally agree. Again, the major discrepancy occurs at 1.0° and the reason is mentioned previously: the 75 V on/off ratio is very sensitive at 1.0°.

The on/off ratios for the 0.5° Y-branch modulator with the two-horn-length electrode are measured on a 3.2 μm waveguide instead of a 4 μm waveguide since the 4 μm one gives multi-mode output. The on/off ratios are in good agreement when the 0.5° branch is operating in single-mode.

Comparing the performance of the two-horn-length modulators with those of three-horn-length, the two-horn-length modulators actually have higher on/off ratios for the 1.5° and 2.0° Y-branch, as predicted by the simulations performed. These results support the fact that a longer electrode does not necessarily increase the on/off ratio and may actually reduce it in some cases.

Chapter VII Recommendations

Although the Y-branch electro-optic modulator can provide high on/off ratios and high percentage guided powers while keeping the electrodes short, e.g., 300 μm long electrode for a 1.5° branch, the switching voltage required is rather high. To reduce this switching voltage, two areas to examine are the Δn_s value and the location of the electrodes. Presumably, the maximum refractive index change Δn_s can be lowered such that the waveguide becomes more weakly guiding, enhancing radiation at 0 V and allowing light to be more easily steered when a voltage is applied. An optimum Δn_s should exist for $0.0035 < \Delta n_s < 0.0042$. Secondly, the placement of the electrode can be optimized so that the electro-optic effect is applied more effectively. One possibility is to shift the electrodes down the horn so that the electrodes begin inside the horn instead of at the beginning of the horn. This could result in shorter electrodes hence giving decreased capacitance and increased device performance.

Improvements can be achieved in the fabrication process. One recommendation is to put more and better designed markers on both the waveguide and electrode masks so that the electrodes can be aligned more precisely. Misalignment not only causes an imbalance of guided power, but more importantly it distorts the on/off ratio.

Another recommendation is to cut and polish the samples prior to patterning the Al electrodes. Since the cutting process and especially the polishing process can easily scratch and damage the electrodes, putting the electrodes on after these fabrication steps should ensure complete electrodes. One suggestion is that after the SiO_2 deposition, a layer of Al would be evaporated onto the samples as a protective layer. Then the samples

would be cut and polished, after which the protective Al layer would be etched away and a new layer of Al would be deposited for patterning of electrodes.

Finally, the development of a high Q resonator to serve as electrodes for the Y-branch should be pursued so that an optical commutator switch may be realized. Since the Y-branch is capable of 10's of GHz switching speed. The commutator switch may prove to be very useful in optical communications.

Chapter VIII Conclusions

We have studied, both theoretically, through numerical simulations, and experimentally, through fabrication and testing, the behaviour of Y-branch electro-optic modulators. The modulator had z-cut $LiNbO_3$ as the substrate, with waveguides formed by the indiffusion of 4 μm wide Ti strips, and electrodes formed by the patterning of Al. The modulator used 632.8 nm light and guided the fundamental TM-like mode. Our goal was to design a Y-branch modulator, with short electrodes, which offers high on/off ratios and high percentage guided powers.

Using the effective index method and the 2-D split-step finite difference beam propagation method, the Y-branch modulator was simulated. During the numerical modelling of the device, a novel way was developed for computing the effective index n_{eff} in non-guiding regions of the waveguide.

From the simulation results, we found that a suitable value of Δn_s can improve the on/off ratio and percentage guided power at any given voltage. This optimum Δn_s was found to be between 0.0035 and 0.0050. In our work, we have chosen to use $\Delta n_s = 0.0042$, which corresponded to a 480Å thick Ti layer for the indiffusion. As for the electrode length, it was found that a two-horn-length electrode gives better performance than a one-horn-length or a three-horn-length electrode. The one-horn-length electrode being too short to cause substantial modulation, and the three-horn-length electrode provided no notable improvement while increasing the device capacitance.

We have also studied the modulator performance as a function of branch angle θ (from 0.5° to 3.0°), and found that in general the on/off ratio increases with increasing

θ while the percentage guided power decreases with increasing θ (at least in regions II and III). Therefore, a compromise must be made between high on/off ratio and high percentage guided power. With voltage application, the on/off ratios increase with all θ. However, the behaviour for the guided power is quite different. For $\theta < 0.8°$ the percentage guided power decreases with voltage. For $\theta > 0.8°$ the percentage guided power actually increases as the applied voltage increases, due to light which is radiated at 0 V being steered into the *ON* branch of the modulator thus adding to the total amount of guided power.

Based on the numerical simulations, our 1.5° Y-branch is expected to have an on/off ratio of 44:1 with a 2 dB loss at 75 V applied voltage, using a two-horn-length electrode of 300 μm long. At this voltage, the device is expected to have a power/unit bandwidth of 1.03 W/GHz, which is the lowest of all the recent modulators.

The Y-branch modulators were fabricated, having branch angles which ranged from 0.5° to 3.0° in 0.5° steps, and two sets of electrodes (two-horn-length and three-horn-length ones). All fabrication parameters were as specified in the simulations. The problem of dust accumulation during fabrication was remedied by minimizing the samples' exposure to open air prior to diffusion. The formation of surface waveguides due to LiO_2 outdiffusion was also overcome. We found that by performing the diffusion in a wet oxygen flow of 1.5 L/min (the O_2 being saturated with water vapour by bubbling through a 7.5" column of water at 80°C), surface waveguiding can be almost if not completely eliminated.

The devices were tested for their on/off ratios and percentage guided power. It was found that in order to obtain the true on/off ratios of the guided mode, an aperture had to be used to reduce the radiation modes. A bulk on/off ratio which included the radiation modes had to be evaluated (via simulations), and it was used to adjust the measured results accordingly so that we could convert the measured bulk on/off ratio to the true on/off ratio of the TM-like guided mode. Using this method of compensation, the experimental values were found to correspond very well to the predictions from the numerical simulations. For example, the 2° Y-branch with the two-horn-length electrode (228 μm) measured an on/off ratio of 59:1 and 47% guided power at 75 V, while the theoretical values were 62:1 and 50% guided power. The on/off ratios showed an increase with branch angle, while the percentage guided powers also decreased with branch angle. More significantly, the percentage guided power indeed increased with applied voltage for $\theta > 0.8°$, and the two-horn-length electrodes in fact performed better than the three-horn-length electrodes.

References

1. R. L. Jungerman, C. Johnsen, D. J. McQuate, K. Salomaa, M. P. Zurakowski, R. C. Bray, G. Conrad, D. Cropper, and P. Hernday , "High-Speed Optical Modulator for Application in Instrumentation,' *IEEE J. Light Tech.*, vol. 8, No.9, pp.1363-1370, September 1990.

2. A. Djupsjöbacka, "Time Division Multiplexing Using Optical Switches," *IEEE J. Select. Areas Commun.*, vol. 6, No. 7, pp.1227-1231, August 1988.

3. P. Granestrand, B. Lagerström, P. Svensson, L. Thylén, B. Stoltz, K. Bergvall, J. E. Falk, and H. Olofsson, "Integrated Optics 4x4 Switch Matrix with Digital Optical Switches," *Electron. Lett.*, vol. 26, No. 1, pp.4-5, January 1990.

4. Y. Silberberg, P. Perlmutter, and J. E. Baran, "Digital Optical Switch," *Appl. Phys. Lett.*, vol. 51, No. 16, pp.1230-1232, October 1987.

5. I. P. Kaminow and L. W. Stulz, "Loss in Cleaved Ti-diffused $LiNbo_3$ Waveguides," *Appl. Phys. Lett.*, vol. 33, No. 1, pp.62-64, July 1978.

6. M. Kondo, Y. Ohta, Y. Tanisawa, T. Aoyama, R. Ishikawa, "Low-Drive-Voltage and Low-Loss-Polarization-Independent $LiNbO_3$ Optical Waveguide Switches," *Electron. Lett.*, vol. 23, No. 21, pp.1167-1169, October 1987.

7. N. A. F. Jaeger, W. C. Lai and M. Chen, US patent pending, "Optical Switch", filed September 1991.

8. W. K. Burns, "Voltage-Length Product for Modal Evolution-Type Digital Switches," *IEEE J. Light. Tech.*, vol. 8, No. 6, pp.990-997, June 1990.

9. R. Baets and P. E. Lagasse, "Calculation of Radiation Loss in Integrated-Optic Tapers and Y-junctions," *Appl. Opt.*, vol. 21, No. 11, pp.1972-1978, June 1982.

10. I. P. Kaminow, L. W. Stulz, and E. H. Turner, "Efficient Strip-waveguide Modulator," *Appl. Phys. Lett.*, vol. 27, No. 10, pp.555-557, November 1975.

11. M. Masuda and J. Koyama, "Effects of a Buffer Layer on TM Modes in a Metal-Clad Optical Waveguide Using Ti-diffused $LiNbO_3$ C-plate," *Appl. Opt.*, vol. 16, No. 11, pp.2994-3000, November 1977.

12. R. V. Schmidt and I. P. Kaminow, " Metal-diffused Optical Waveguides in $LiNbO_3$," *Appl. Phys. Lett.*, vol. 25, No. 8, pp.458-460, October 1974.

13. M. Minakata, S. Saito, M. Shibata and S. Miyazawa, "Precise Determination of Refractive-index Changes in Ti-diffused $LiNbO_3$ Optical Waveguides," *J. Appl. Phys.*, vol. 49, No. 9, pp.4677-4682, September 1978.

14. M. Minakata, S. Saito and M. Shibata, "Two-dimensional Distribution of Refractive-index Changes in Ti-diffused $LiNbO_3$ Strip Waveguides," *J. Appl. Phys.*, vol. 50, No. 5, pp.3063-3067, May 1979.

15. G. B. Hocker and W. K. Burns, "Mode Dispersion in Diffused Channel Waveguides by the Effective Index Method," *Appl. Opt.*, vol.16, No. 1, pp.113-118, January 1977.

16. R. J. Holmes and D. M. Smyth, "Titanium Diffusion into $LiNbO_3$ as a Function of Stoichiometry," *J. Appl. Phys.*, vol. 55, No. 10, pp.3531-3535, May 1984.

17. E. Yamashita, editor, *Analysis Methods for Electromagnetic Wave Problems,* Artech House, 1990.

18. Working Group I, COST 216, "Comparison of Different Modelling Techniques for Longitudinally Invariant Integrated Optical Waveguides," *IEE Proc.*, vol. 136, No. 5, pp.273-280, October 1989.

19. G. B. Hocker and W. K. Burns, "Modes in Diffused Optical Waveguides of Arbitrary Index Profile," *IEEE J. Quantum Electron.*, vol. 11, No. 6, pp.270-276, June 1975.

20. D. Yevick and B. Hermansson, "Split-Step Finite Difference Analysis of Rib Waveguides," *Electron. Lett.*, vol. 25, No. 7, pp.461-462, March 1989.

21. J. Saijonmaa and D. Yevick, "Beam-propagation analysis of loss in bent optical waveguides and fibers," *J. Opt. Soc. Am.*, vol. 73, No. 12, pp.1785-1791, December 1983.

22. N. A. F. Jaeger and L. Young, "Voltage-Induced Optical Waveguide Modulator in Lithium Niobate," *IEEE J. Quantum Electron.*, vol. 25, No. 4, pp.720-728, April 1989.

23. R. Keil and F. Auracher, "Coupling of Single-mode Ti-diffused $LiNbO_3$ Waveguide to Single-mode Fibers," *Optics Comm.*, vol. 30, No. 1, pp. 23-28, July 1979.

24. D. Marcuse, *Light Transmission Optics*. 2nd ed. New York: Van Nostrand Rienhold, 1982.

25. D. Yevick and P. Danielsen, "Numerical Investigation of Mode Coupling in Sinusoidally Modulated GRIN Planar Waveguides," *Appl. Opt.*, vol. 21, No. 15, pp.2727-2733, August 1982.

26. M. D. Feit and J. A. Fleck, Jr., "Computation of Mode Properties in Optical Fiber Waveguides by a Propagating Beam Method," *Appl. Opt.*, vol. 19, No. 17, pp.1154-1164, April 1980.

27. K. T. Koai and P. Liu, "Modeling of Ti:LiNbO$_3$ Waveguide Devices: Part I - Directional Couplers," *IEEE J. Light. Tech.*, vol. 7, No. 3, pp.533-539, March 1989.

28. W. C. Lai, "The Effects of Branch Angle on a Y-branch Optical Modulator," *The First Graduate Student Conference on Opto-Electronics Materials, Devices, and Systems*, pp.30, McMaster University, Hamilton, Ontario, June 24-26, 1991.

29. Personal communication with A. Doty at Tektronics, Inc.

30. A. Imani, A. Luey, and T. Ngo, "Voltage Steered Integrated Optical Y-branch Modulator," Systems Lab Report, Department of Electrical Engineering, University of British Columbia, February 1990.

31. J. Feng and H. Seto, "Fabrication and Testing of Y-branch Switches," Systems Lab Report, Department of Electrical Engineering, University of British Columbia, January 1991.

32. J. L. Jackel, "Suppression of Outdiffusion in Titanium Diffused LiNbO$_3$: A Review," *J. Opt. Comm.*, vol. 3, No. 3, pp.82-85, 1982.

33. M. N. Armenise, "Fabrication Techniques of Lithium Niobate Waveguides," *IEE Proc.*, vol. 135, No. 2, pp.85-91, April 1988.

34. A. Neyer and T. Pohlmann, "Fabrication of Low-Loss Titanium-Diffused LiNbO$_3$ Waveguides using a Closed Platinum Crucible," *Electron. Lett.*, vol. 23, No. 22,

pp.1187-1188, October 1987.

35. R. J. Esdaile, "Closed-tube Control of Out-diffusion during Fabrication of Optical Waveguides in LiNbO$_3$," *Appl. Phys. Lett.,* vol. 33, No. 8, pp.733-734, October 1978.

36. J. L. Jackel, V. Ramaswamy, and S. P. Lyman, "Elimination of Out-diffused Surface Guiding in Titanium-diffused LiNbO$_3$" *Appl. Phys. Lett.,* vol. 38, No. 7, pp.509-511, April 1981.

37. M. De Sario, M. N. Armenise, C. Canali, A. Carnera, P. Mazzoldi, and G.Celotti, "TiO$_2$, LiNb$_3$O$_8$, and (Ti$_x$Nb$_{1-x}$)O$_2$ Compound Kinetics during Ti:LiNbO$_3$ Waveguide Fabrication in the Presence of Water Vapors," *J. Appl. Phys.,* vol. 57, No. 5, pp.1482-1488, March 1985.

38. S. Forouhar, G. E. Betts, and W. S. C. Chang, "Effects of Water Vapor on Modes in Ti-indiffused LiNbO$_3$ Planar Waveguides," *Appl. Phys. Lett.,* vol. 45, No. 3, pp.207-209, August 1984.

39. C. Canali, C. De Bernardi, M. De Sario, A. Loffredo, G. Mazzi, and S.Morasca, "Effects of Water Vapor on Refractive Index Profiles in Ti:LiNbO$_3$ Planar Waveguides," *IEEE J. Light. Tech.,* vol. 4, No. 7, pp.951-955, July 1986.

40. N. A. F. Jaeger and W. C. Lai, "Y-branch Optical Modulator," *SPIE OE/FIBRES'91 Proc.,* Boston, Massachusetts, USA, September 3-6 1991.

41. O. G. Ramer, "Integrated Optic Electrooptic Modulator Electrode Analysis," *IEEE J Quantum Electron.,* vol. 18, No. 3, March 1982.

42. S. K. Korotky, W. J. Minford, L. L. Buhl, M. D. Divino, and R. C. Alferness, "Mode Size and Method for Estimating the Propagation Constant of Single-mode Ti:LiNbO$_3$ Strip Waveguides," *IEEE J. Quantum Electron.*, vol. 18, No. 10, October 1982.

Appendix A Calculation of Modulator Capacitance and Power Requirement

According to Kaminow, Stulz and Turner [10], the capacitance of coplanar electrodes on a dielectric slab with dielectric constant ϵ_s surrounded by a medium with dielectric constant ϵ_m is approximately

$$C = (\epsilon_o/\pi)(\epsilon_s + \epsilon_m) L \ln(4w_2/w_1) \qquad (A.1)$$

for $(w_1/w_2)^2 << 1$. L is the electrode length, w_1 and w_2 are the spacings between the inner and outer edges of the electrodes respectively, and ϵ_0 is the vacuum permittivity. The surrounding dielectric constant ϵ_m is 1 for air, and ϵ_s for LiNbO$_3$ is the average value of the principal dielectric constants $\epsilon_a = 43$ and $\epsilon_c = 28$.

Our two-horn-length electrode device has an average gap width of 5 μm (since it has a 4 μm gap for one-horn-length, and a 4-to-8 μm gap for the second horn-length). We assume an electrode width five times that of the gap width since Ramer [41] has shown that the electric field distribution for such a coplanar electrode is almost identical to that of a semi-infinite electrode. Therefore $w_1 = 5$ μm, and $w_2 = 5\times5 + 5\times5 + 5 = 55$ μm, and $(w_1/w_2)^2 << 1$ holds. Using $L = 300$ μm for the 1.5° device, the calculated capacitance is 0.117 pF.

The 3 dB bandwidth can be evaluated from $\Delta f = 1/(\pi RC)$. If a matching resistance of 50 Ω is assumed, then a 3 dB bandwidth of 54.4 GHz is obtained.

The power per unit bandwidth is

$$P/\Delta f = \pi(CV^2/2) \qquad (A.2)$$

where C is the capacitance, and V is the peak modulating voltage. Using $C = 0.117$ pF

and $V = 75$ V, the power per unit bandwidth is 1.03 W/GHz.

The (w_2/w_1) value is assumed to be a constant for all devices $((w_2/w_1) = 11)$, so the only variables in computing $P/\Delta f$ are the electrode length L and the applied voltage V and (A.2) becomes

$$P/\Delta f = (\epsilon_o/2)(\epsilon_s + \epsilon_m)\ln(4w_2/w_1)\,L\,V^2 \qquad\qquad \text{(A.3)}$$

For Silberberg's device [4], $L = 1.5$ cm and $V = 15$ V, hence having 2.06 W/GHz. Granestrand's device [3] has $L = 0.57$ cm and $V = 60$ V, thus giving a power of 12.5 W/GHz. The directional coupler [6] has $L = 1.9$ cm and $V = 18$ V, and therefore 3.76 W/GHz.

Appendix B Calculation of Δn_s from Titanium Thickness

Based on the assumed diffusion distribution (equation 3.1 (a)) and the conservation of atoms, the maximum refractive index change due to diffusing a metal of thickness τ into a substrate is [42]

$$\Delta n = \frac{dn}{dc}\, erf\left(\frac{W}{2\sqrt{2D}}\right)\sqrt{\frac{2}{\pi}}\left(\frac{\tau}{D}\right) \qquad\qquad (B.1)$$

D is the diffusion depth ($D = 2(Dt)^{1/2}$, t is time, and D, the diffusion temperature coefficient, is 1.06×10^{-12} cm^2/s at 1050°C for a congruent composition of 48.6 mol % LiO$_2$ [16]), W is the width of the Ti strip prior to diffusion, and (dn/dc) is the change in index per unit change in metal concentration. For LiNbO$_3$ at 632.8 nm, the $(dn/dc)_e$ for the extraordinary polarized light is reported to be 0.76 by Koai and Pui [27] and 0.625 by Minakata et al. [13]. Here we use the average value of the two, i.e., $(dn/dc)_e = 0.6925$. Using $W = 4$ μm and $t = 6$ hours in (B.1), the Ti thickness required for a maximum refractive change of 0.0042 is 480Å.